## **IMMUNE REGULATION**

## A helminth enzyme subverts macrophage-mediated immunity by epigenetic targeting of prostaglandin synthesis

Sina Bohnacker<sup>1,2</sup>, Fiona D. R. Henkel<sup>2</sup>†, Franziska Hartung<sup>2</sup>†, Arie Geerlof<sup>3</sup>, Sandra Riemer<sup>2</sup>, Ulrich F. Prodjinotho<sup>4,5,6</sup>, Eya Ben Salah<sup>1</sup>, André Santos Dias Mourão<sup>3</sup>, Stefan Bohn<sup>7,8</sup>, Tarvi Teder<sup>9</sup>, Dominique Thomas<sup>10,11</sup>, Robert Gurke<sup>10,11</sup>, Christiane Boeckel<sup>12</sup>, Minhaz Ud-Dean<sup>12</sup>, Ann-Christine König<sup>13</sup>, Alessandro Quaranta<sup>14</sup>, Francesca Alessandrini<sup>2</sup>, Antonie Lechner<sup>2</sup>, Benedikt Spitzlberger<sup>2</sup>, Agnieszka M. Kabat<sup>15</sup>‡, Edward Pearce<sup>15</sup>, Jesper Z. Haeggström<sup>9</sup>, Stefanie M. Hauck<sup>13</sup>, Craig E. Wheelock<sup>14,16</sup>, Per-Johan Jakobsson<sup>17</sup>, Michael Sattler<sup>8,18</sup>, David Voehringer<sup>19</sup>, Matthias J. Feige<sup>20</sup>, Clarissa Prazeres da Costa<sup>4,5,6</sup>, Julia Esser-von Bieren<sup>1,2</sup>\*

The molecular mechanisms by which worm parasites evade host immunity are incompletely understood. In a mouse model of intestinal helminth infection using *Heligmosomoides polygyrus bakeri* (*Hpb*), we show that helminthic glutamate dehydrogenase (heGDH) drives parasite chronicity by suppressing macrophage-mediated host defense. Combining RNA-seq, ChIP-seq, and targeted lipidomics, we identify prostaglandin E<sub>2</sub> (PGE<sub>2</sub>) as a major immune regulatory mechanism of heGDH. The induction of PGE<sub>2</sub> and other immunoregulatory factors, including IL-12 family cytokines and indoleamine 2,3-dioxygenase 1, by heGDH required p300-mediated histone acetylation, whereas the enzyme's catalytic activity suppressed the synthesis of type 2–promoting leukotrienes by macrophages via 2-hydroxyglutarate. By contrast, the induction of immunoregulatory factors involved the heGDH N terminus by potentially mediating interactions with cellular targets (CD64 and GPNMB) identified by proteomics. Type 2 cytokines counteracted suppressive effects of heGDH on host defense, indicating that type 2 immunity can limit helminth-driven immune evasion. Thus, helminths harness a ubiquitous metabolic enzyme to epigenetically target type 2 macrophage activation and establish chronicity.

# Copyright © 2024 The Authors, some rights reserved; exclusive licensee American Association for the Advancement of Science. No claim to original U.S. Government Works

### INTRODUCTION

More than 1000 different parasites can infect humans, and approximately one-third of the human population worldwide is infected with worm parasites (helminths) (1, 2). During evolution, helminths have developed survival strategies to suppress host defenses and establish chronic infections. Given the mechanistic similarities between antihelminth immunity and type 2 inflammatory diseases (e.g., asthma), immune evasion strategies of parasitic helminths can potentially be exploited therapeutically (3). However, the mechanisms and molecules by which helminths control antiparasitic immune responses so as to persist in the host are largely unknown.

Protective immunity against helminth parasites often relies on the induction of a type 2 immune response characterized by the production of type 2 cytokines that activate host effector cells such as macrophages, granulocytes, and T helper 2 ( $T_{\rm H}2$ ) cells (4–9). Helminths can efficiently suppress this type 2 immune response by targeting cytokines [e.g., interleukin-33 (IL-33)] important for its induction (10) or by inducing regulatory T cells ( $T_{\rm regs}$ ) and tolerogenic macrophages (11).

We have previously shown that larval products containing the glutamate dehydrogenase (GDH) of the rodent nematode parasite *Heligmosomoides polygyrus bakeri* (*Hpb*) suppress allergic inflammation in a mouse model of asthma and induce a shift in the arachidonic acid (AA) metabolic pathway (*12*). AA metabolites can act as bioactive derivatives with key roles in infection and inflammation (*13*). Leukotrienes (LTs) synthesized by 5-lipoxygenase (5-LOX) promote

<sup>1</sup>Department of Immunobiology, Université de Lausanne, Epalinges, Switzerland. <sup>2</sup>Center of Allergy and Environment (ZAUM), Technical University of Munich and Helmholtz Munich, German Research Center for Environmental Health, Munich, Germany. <sup>3</sup>Protein Expression and Purification Facility (PEPF), Institute of Structural Biology, Helmholtz Munich, German Research Center for Environmental Health, Neuherberg, Germany. <sup>4</sup>Institute for Microbiology, Immunology and Hygiene, Technical University of Munich, Munich, Germany. <sup>5</sup>Cerman Center for Infection Research (DZIF), Munich, Germany. <sup>7</sup>Department of CryoEM Technology, Max Planck Institute of Biochemistry, Martinsried, Germany. <sup>8</sup>Ceryo-Electron Microscopy Platform and Institute of Structural Biology, Helmholtz Munich, German Research Center for Environmental Health, Neuherberg, Germany. <sup>9</sup>Department of Medical Biochemistry and Biophysics, Division of Chemistry II, Karolinska Institute, Stockholm, Sweden. <sup>10</sup>Institute of Clinical Pharmacology, Faculty of Medicine, Goethe University Frankfurt, Frankfurt am Main, Germany. <sup>11</sup>Fraunhofer Institute for Translational Medicine and Pharmacology (ITMP) and Fraunhofer Cluster of Excellence for Immune Mediated Diseases (CIMD), Frankfurt am Main, Germany. <sup>12</sup>Institute of Computational Biology, Helmholtz Munich, German Research Center for Environmental Health, Neuherberg, Germany. <sup>13</sup>Metabolomics and Proteomics Core, Helmholtz Munich, German Research Center for Environmental Health, Neuherberg, Germany. <sup>14</sup>Unit of Integrative Metabolomics, Institute of Environmental Medicine, Karolinska Institute, Stockholm, Sweden. <sup>15</sup>Max Planck Institute for Immunobiology and Epigenetics, Freiburg, Germany. <sup>16</sup>Department of Respiratory Medicine and Allergy, Karolinska University Hospital at Solna, Stockholm, Sweden. <sup>18</sup>Bavarian NMR-Center, Department of Medicine, Division of Rheumatology, Karolinska Institute for Bioscience, TUM School of Natural Sciences, Technical University of Munich, Germany.

<sup>\*</sup>Corresponding author. Email: julia.esser-vonbieren@unil.ch

<sup>†</sup>These authors contributed equally to this work.

<sup>‡</sup>Present address: Novartis Biomedical Research, 4056 Basel, Switzerland.

type 2 inflammation and helminth expulsion (14, 15). By contrast, prostaglandins synthesized by the cyclooxygenase (COX) pathway show both type 2–promoting (16, 17) and type 2–suppressive capacities (18–20) during allergic airway inflammation or infections with helminth parasites. GDHs are widely conserved among parasitic helminths, including the human cestode parasite *Taenia solium* (Ts), in which GDH was shown to drive  $T_{regs}$  by up-regulating the immunoregulatory AA metabolite prostaglandin  $E_2$  (PGE<sub>2</sub>) (18). However, it remained unclear how helminthic GDH (heGDH) can modulate AA metabolic pathways and whether this would promote immune evasion and parasite chronicity. Hpb is a natural parasite of mice and establishes chronic infections in the small intestine, starting with the ingestion of infective (L3) larvae that develop into a juvenile tissue stage (L4) and adult (L5) worms that mate and produce eggs within the intestinal lumen.

Here, we demonstrate that heGDH enables parasite chronicity by targeting macrophages. Upon internalization, heGDH regulates macrophage tricarboxylic acid (TCA) and amino acid metabolism to suppress LTs via its catalytic activity, whereas its noncatalytic N terminus activates the p300 histone acetyltransferase (HAT) to induce the expression of multiple immune regulatory genes, including PGE2 synthetic enzymes. The heGDH-mediated induction of myeloid PGE2 synthesis suppresses alternative macrophage activation and  $T_{\rm H2}$  activation essential for host defense, thus identifying heGDH as a key factor of helminthic immune evasion.

### **RESULTS**

## GDH enables helminth immune evasion by inducing type 2-suppressive macrophages

We previously identified GDH as a helminth-derived factor able to suppress type 2 inflammation in a mouse model of allergic asthma (12). However, the evolutionary role of GDH during helminth infection remained elusive. heGDH is expressed by all stages of the murine intestinal nematode parasite Hpb, with higher levels [lower threshold cycle (Ct) value] found in the infectious L3 stage as compared with the juvenile (L4) or the adult (L5) stages (fig. S1A). To investigate whether GDH is essential for parasite immune evasion, we treated Hpb-infected mice with a specific neutralizing monoclonal antibody (mAb; clone 4F8) against heGDH (Fig. 1A) (12). When first infecting its host, Hpb causes a chronic infection with adult (L5) worm counts peaking around 2 weeks postinfection (p.i.). mAb (4F8)–mediated neutralization of heGDH resulted in lower worm counts 14 days p.i. (Fig. 1B), suggesting that heGDH is a key factor in the Hpb-mediated suppression of type 2 immunity.

Macrophages are essential players in host defense against parasite infections (21), and recruited bone marrow–derived macrophages (BMDMs) and/or monocyte-derived macrophages (MDMs) are particularly important for antihelminth immunity (8). 4F8 treatment did not affect the accumulation of CD64<sup>+</sup> macrophages or Alox15<sup>+</sup> cells (mostly eosinophils) (22), whereas neutrophils (MPO<sup>+</sup>) tended to increase in the granulomas of *Hpb*-infected mice at the peak of infection (fig. S1B). Immunofluorescence (IF) staining using the 4F8 antibody revealed colocalization of heGDH with CD64<sup>+</sup> macrophages near *Hpb* larvae in the small intestinal submucosa early during infection (Fig. 1C and fig. S1C). Stimulation of human MDMs or murine BMDMs with recombinant heGDH resulted in binding and uptake of the protein, which was detectable for at least 24 hours in the cytoplasm (Fig. 1D and fig. S1, D and E).

To further define the immune regulatory effects of heGDH, RNA sequencing (RNA-seq) was performed, revealing broadly altered transcriptional profiles of heGDH-treated compared with control-treated MDMs. In particular, heGDH increased the expression of immunoregulatory and type 2-suppressive genes, including IDO1, PTGES [microsomal prostaglandin E synthase-1 (mPGES-1)], PTGS2 (COX2), PTGIR, IL12B, and EBI3 (Fig. 1, E and F) (23-28). To exclude that the heGDH-triggered induction of regulatory mediators was due to endotoxin contamination, we compared the transcriptional profiles of MDMs stimulated with heGDH with MDMs stimulated with lipopolysaccharide (LPS) at the concentration present in the preparation of heGDH (0.5 to 1 ng/ml) (fig. S2, A and B). Although low-dose (1 ng/ml) LPS up-regulated several genes and mediators (fig. S2, C and D) that were induced by heGDH, MDMs stimulated with heGDH showed a much stronger induction of the same top differentially expressed genes (DEGs) (fig. S2, A and B), confirming that heGDH imprints a type 2–suppressive macrophage phenotype independent of the low amounts of contaminating LPS. In line with the increased expression of genes involved in prostanoid synthesis and signaling, heGDH dose-dependently increased PGE2 and IL-10 production by human MDMs (fig. S3A). Broader liquid chromatography-tandem mass spectrometry (LC-MS/MS) analysis of AA metabolites revealed a shift from type 2-inducing metabolites (cysteinyl leukotrienes, cysLTs) to mediators involved in tissue repair and immune regulation [prostaglandin D2 (PGD<sub>2</sub>), PGE<sub>2</sub>, thromboxane (TX)B<sub>2</sub>, and IL-10] (29, 30) in heGDH-treated MDMs, when compared with phosphatebuffered saline (PBS)-stimulated cells (Ctrl) or cells treated with a "mock vector" control (i.e., an Escherichia coli lysate undergoing the same purification steps as the recombinant protein) (Fig. 2, A to C). Thus, eicosanoid modulatory effects of recombinant heGDH were not due to potential bacterial contaminants. Neutralization with clone 4F8 partially abrogated the heGDH-mediated regulation of IL-10 and COX-2 to a similar extent as previously observed for crude L3 extract (fig. S3, B and C) (12). In contrast, 4F8 could not prevent or reverse the heGDH-mediated suppression of 5-LOX metabolites (fig. S3D), suggesting distinct mechanisms for the modulation of immune regulatory and reparative mediators on the one hand and type 2-promoting mediators (LTs) on the other hand. Together, these data suggest that heGDH suppresses antihelminth host defense by broadly modulating macrophage effector functions.

## p300 HAT activation by heGDH mediates the induction of immune regulatory genes

Multiple regulatory genes induced by heGDH, including PGE2 synthetic enzymes and *IL12B*, are known to be regulated via p300 histone acetyl transferase (HAT) (Fig. 1E and fig. S2A) (31–33), which suggested an epigenetic mechanism of action. Addition of a p300/CBP HAT inhibitor, A485, during treatment with heGDH resulted in suppression of the top DEGs identified by RNA-seq (IL12B, IDO1, PTGS2, EBI3, and PTGES), whereas the heGDHtriggered induction of interferon-stimulated genes remained unaffected (Fig. 3A and fig. S4, A and B). Decreased gene expression correlated with a strongly diminished secretion of PGE<sub>2</sub>, IL-12β (p40), and IL-10 in heGDH-stimulated macrophages treated with the p300 HAT inhibitor (Fig. 3B), which was not due to cellular toxicity (fig. S4C). Knockdown of p300 during heGDH stimulation by small interfering RNA (siRNA; fig. S4D) confirmed the p300-dependent induction of target proteins, including COX-2 and mPGES-1 in MDMs and BMDMs (Fig. 3C and fig. S4E),

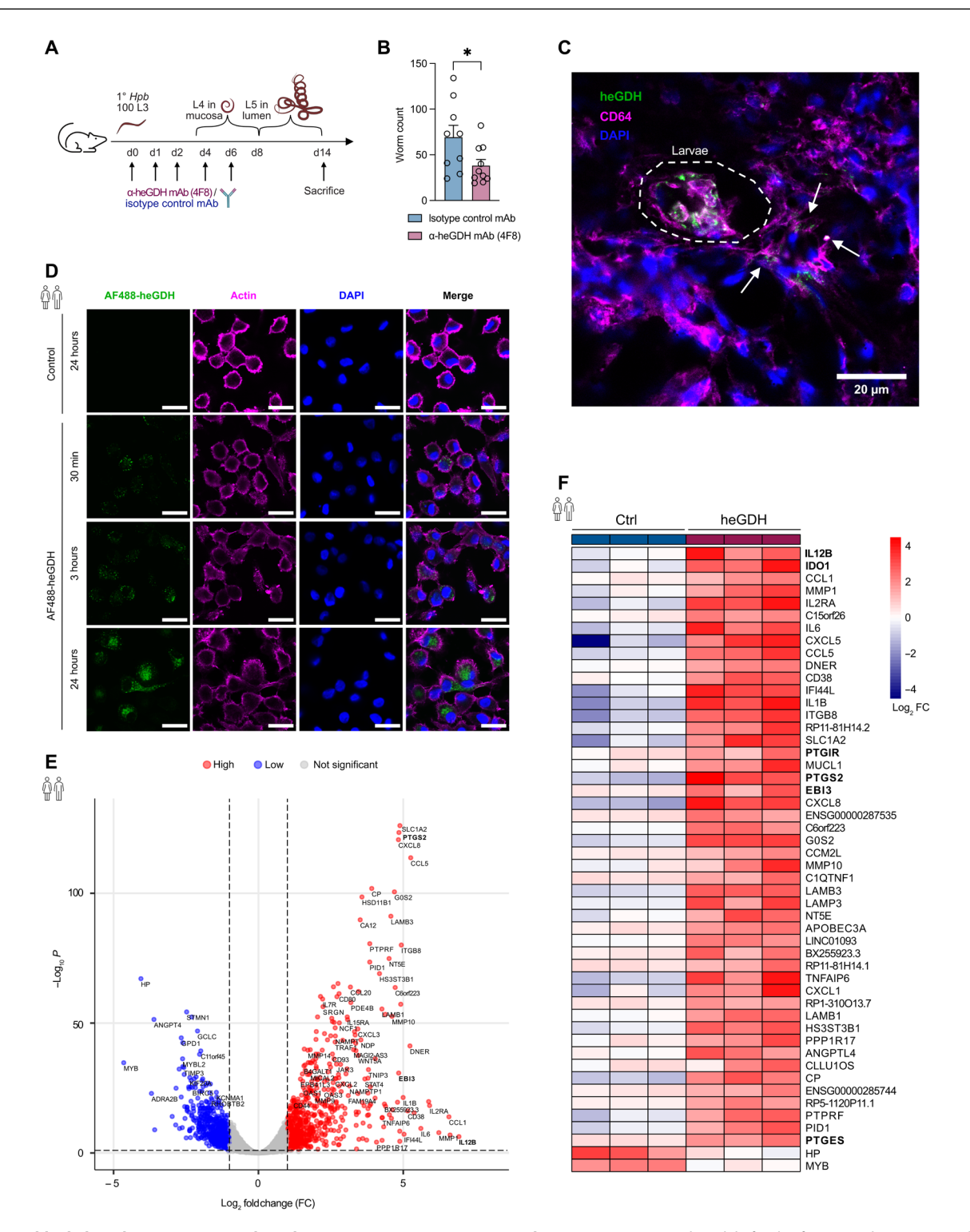


**Fig. 1. GDH enables helminth immune evasion by inducing type 2–suppressive macrophages.** (**A**) Experimental model of Hpb infection and treatment with α-heGDH mAb (4F8) or isotype control antibody. d0, day 0. (**B**) Worm burden 14 days p.i. in mice treated with 10 μg α-heGDH mAb or isotype control (n = 9) in the isotype control mAb group; n = 10 in the α-heGDH mAb group). (**C**) Representative IF image for heGDH (green), CD64 (magenta), and DAPI (blue) in the small intestine from a mouse infected with Hpb (4 days). White arrows indicate colocalization of heGDH and macrophages in the surroundings of L4 larvae (dashed circle). (**D**) Representative IF images for human MDMs  $\pm$  treatment with AF488-labeled heGDH (5 μg/ml; green), actin (magenta), and DAPI (blue) for different time points. Scale bars, 20 μm. (**E**) Volcano plot showing DEGs for MDMs  $\pm$  heGDH (5 μg/ml; n = 3 donors). Significant DEGs were selected by a base mean > 50, Padj < 0.1, and  $log_2 FC > 1$ . Labeled DEGs selected with  $Padj < 1 \times 10^{-20}$  or  $log_2 FC > 4$ . (**F**) Heatmap showing top 50 DEGs of MDMs treated  $\pm$  heGDH (5 μg/ml; n = 3 donors). Data are pooled from at least two independent experiments and presented as means + SEM. Statistical significance was determined by Mann-Whitney test (B) or DESeq2 (E and F). \*P < 0.05 (B).

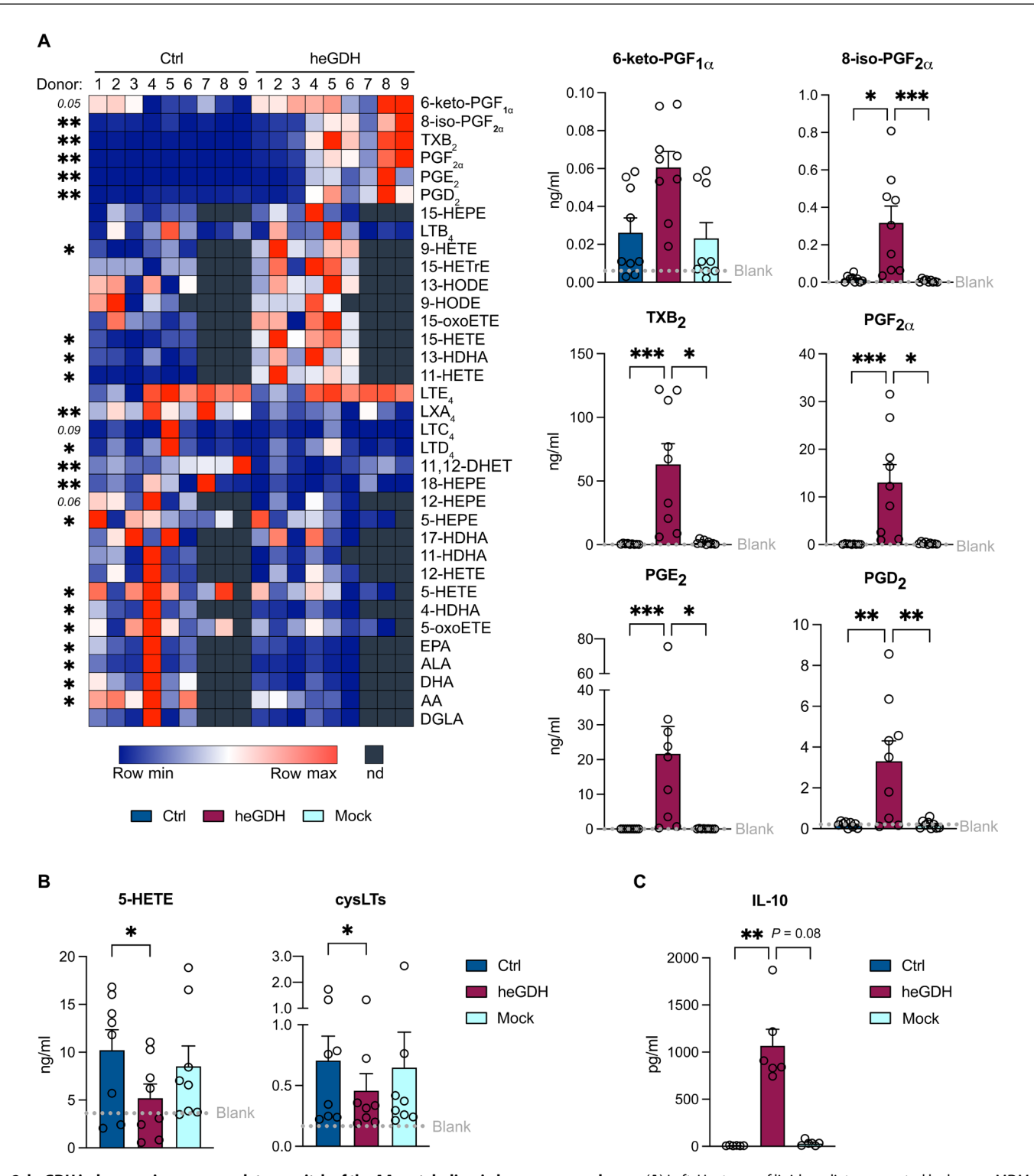
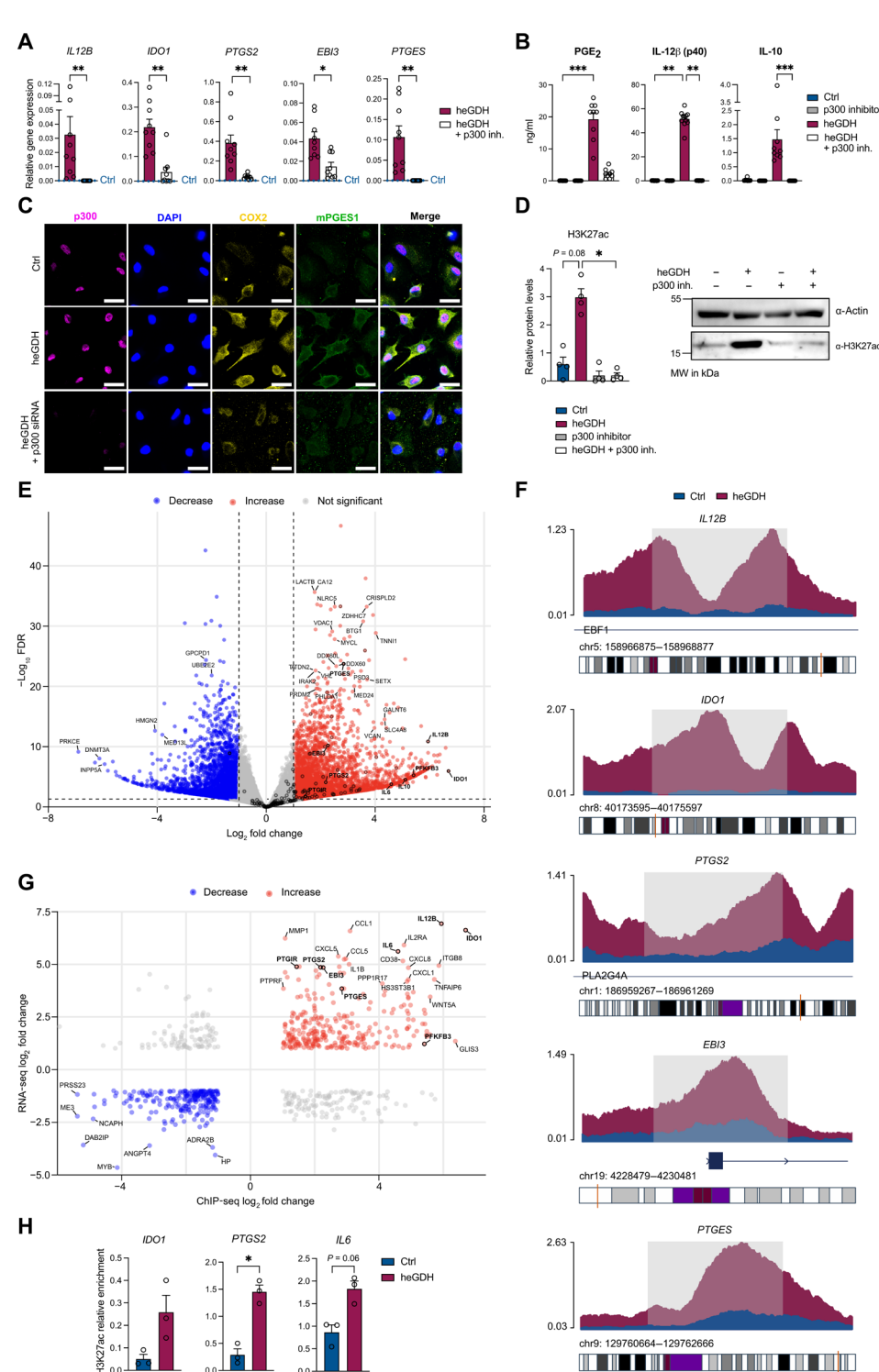


Fig. 2. heGDH induces an immune regulatory switch of the AA metabolism in human macrophages. (A) Left: Heatmap of lipid mediators secreted by human MDMs  $\pm$  treatment with heGDH (5  $\mu$ g/ml; LC-MS/MS). nd, not detected. Right: Concentrations of major COX metabolites produced by human MDMs  $\pm$  heGDH (5  $\mu$ g/ml) or mock vector purification (n=9 donors). Blank, medium control. (B) Major 5-LOX metabolites (LC-MS/MS) released by human MDMs  $\pm$  heGDH (5  $\mu$ g/ml) or mock vector purification (n=8 donors). Blank, medium control. (C) Secretion of IL-10 (ELISA) by MDMs  $\pm$  heGDH (5  $\mu$ g/ml) or mock vector purification (n=6 donors). Data are pooled from at least two independent experiments and presented as means + SEM. Statistical significance was determined by Wilcoxon test [(A), heatmap)] and Friedman test [(A) to (C), bar graphs]. \*P < 0.05, \*\*P < 0.01, and \*\*\*P < 0.001.

Fig. 3. p300 HAT activation by heGDH mediates the induction of immune regulatory genes. (A) Gene expression analysis of top DEGs (qPCR) in MDMs + heGDH (5  $\mu$ g/ml)  $\pm$  6.6  $\mu$ M p300 HAT inhibitor (inh., A485) (n = 9 donors). Dotted lines indicate expression in control (Ctrl) cells. (B)  $PGE_2$  (n = 9donors), IL-12 $\beta$  (n = 11 donors), and IL-10 (n = 10donors) secretion (ELISA) from MDMs ± heGDH  $(5 \mu g/ml) \pm 6.6 \mu M p300 HAT inhibitor (A485).$ (C) Representative IF images of p300 (magenta), DAPI (blue), COX2 (yellow), and mPGES1 (green) in MDMs  $\pm$  heGDH (5  $\mu$ g/ml; Ctrl or p300 knockdown). Scale bars, 20 µm. (D) H3K27ac or actin (protein immunoblot) in MDMs  $\pm$  heGDH (5  $\mu$ g/ml)  $\pm$ 6.6 µM p300 HAT inhibitor (A485). Left: Quantification for n = 4 donors. Right: Representative blot for one donor. MW, molecular weight. (E) H3K27ac peaks for MDMs  $\pm$  heGDH (5  $\mu$ g/ml; n = 3 donors). Colored: FDR  $\leq$  0.05; absolute  $\log_2$  FC > 1. Peaks of top hits from RNA-seq marked (black dots); bold: most significant peak. Further labeled peaks: overlapping hits from ChIP-and RNA-seq. (F) Average H3K27ac ChIP-seq signal of MDMs ± heGDH (5 μg/ ml; n = 3 donors) for top differential peaks (gray window; FDR  $\leq$  0.05; absolute  $\log_2 FC > 1$ ). (**G**) Scatterplot showing top DEGs from RNA-seq against the top H3K27ac peaks from ChIP-seq. Genes of interest marked black and bold. (H) H3K27ac ChIPqPCR for IDO1, PTGS2, and IL6 in MDMs ± heGDH (5  $\mu$ g/ml; n = 3 donors). Data are pooled from at least two independent experiments and presented as means + SEM. Statistical significance was determined by Wilcoxon test (A), Friedman test (B), RM one-way ANOVA (D), or paired t test (H). \*P < 0.05, \*\**P* < 0.01, and \*\*\**P* < 0.001.



whereas CD64 remained unaffected (fig. S4F). In line with the heGDH-mediated activation of p300, global heGDH-induced histone H3 lysine 27 acetylation (H3K27ac) was abrogated by p300 inhibition (Fig. 3D and fig. S4G). H3K27ac enrichment in enhancer regions of heGDH-treated MDMs was confirmed by chromatin immunoprecipitation sequencing (ChIP-seq) analysis, showing a large

intersection between H3K27ac peaks and top DEGs from RNA-seq (Fig. 3, E to G). Assessment of the linear relationship between ChIP-seq and RNA-seq values across genes revealed a weak but highly significant positive correlation (r = 0.16,  $P = 2.2 \times 10^{-16}$ ), suggesting a robust association between ChIP-seq and RNA-seq values across genes. An overall overlap between both datasets was also apparent for

eicosanoid synthesis pathways (fig. S4H). Targeted ChIP-quantitative polymerase chain reaction (qPCR) analysis of H3K27ac for *IDO1*, *PTGS2*, and *IL6* further confirmed this enrichment (Fig. 3H), supporting a key role for p300-mediated H3K27ac in immunoregulation by heGDH.

## Noncatalytic features rather than the catalytic activity of heGDH confer its immune regulatory functions

To discern whether immunoregulation by heGDH depends on the enzyme's catalytic activity or its noncatalytical features, we combined site-directed mutagenesis and structure elucidation by cryo-electron microscopy single-particle analysis (cryo-EM SPA) and x-ray crystallography (fig. S5, A to C). GDH is a hexameric enzyme that catalyzes the reversible conversion of glutamate to  $\alpha$ -ketoglutarate ( $\alpha$ -KG) and ammonia while reducing nicotinamide adenine dinucleotide phosphate [NAD(P)<sup>+</sup>] to the reduced form of NADP<sup>+</sup> [NAD(P)H]. An enzymatic assay revealed α-KG, glutamate, and ammonium as sole substrates and optimum pH values at 8.5 for glutamate utilization and 7.5 for glutamate formation as well as specificity for nicotinamide adenine dinucleotide (NAD<sup>+</sup>)/reduced form of NAD<sup>+</sup> (NADH) as cofactors (fig. S6, A to C). Guanosine triphosphate (GTP), an allosteric GDH inhibitor or bithionol, which is also used as an antihelminthic, reduced the activity of heGDH (fig. S6D). In contrast, clone 4F8 failed to inhibit heGDH catalytic activity (fig. S6E) as well as LT suppression (fig. S3D) while attenuating the heGDH-mediated induction of the COX pathway (fig. S3B). This suggested that noncatalytical features of heGDH are responsible for the induction of immune regulatory and tissue reparative prostanoids.

To untangle the role of catalytic activity versus noncatalytical properties, we designed a catalytically inactive mutant of heGDH (heGDH<sup>K126A, D204N</sup>) (Fig. 4A) (*34*). This mutant still induced COX metabolite and IL-10 production by macrophages to an equivalent or higher degree compared with the wild-type protein (Fig. 4, B and C, and fig. S6F). Gene expression data confirmed a similar or even stronger response of the top DEGs upon stimulation with mutant heGDH<sup>K126A, D204N</sup> (Fig. 4D). In contrast to its effects on prostanoids, heGDH<sup>K126A, D204N</sup> failed to significantly suppress cysLTs (Fig. 4E), supporting the hypothesis that the heGDH-driven induction of the COX pathway via p300 is mediated via noncatalytic features, whereas the catalytic function is necessary to reduce LT production. A role for the catalytic activity in the suppressive effects on LTs was supported by a similar or even stronger reduction of cysLT formation by distinct helminthic (*Ts*) or human GDH (Fig. 4F and fig. S6G).

## heGDH induces regulatory mediators via its N terminus

Cryo-EM and x-ray crystallography of heGDH yielded similar structures with a D3 symmetry (Fig. 5A) and a resolution at 2.7 and 1.8 Å, respectively, resembling the overall architecture of mammalian GDH (fig. S7A). Unlike its mammalian counterparts or the x-ray model (fig. S7, A and B), the cryo-EM density of heGDH contains three "handle"-like densities in the central symmetry plane, each connecting two monomers (Fig. 5, A and B). These handle-like densities, with the size and shape of a short  $\alpha$  helix or a small unstructured region, connect to the side chain density of Cys<sup>136</sup> and are in close proximity to the N-terminal tails of heGDH as identified by x-ray crystallography (Fig. 5B). The handles and N termini are exposed to the exterior solvent and may provide an ideal docking site for interaction partners of heGDH. To decipher the role of these non-catalytical features in heGDH-driven immune regulation, effects of

a mutant lacking the handle-like densities (heGDH<sup>C136S</sup>) (Fig. 5C and fig. S7C) or the N terminus (heGDH<sup> $\Delta N$ </sup>) (Fig. 5C and fig. S7D) were compared with the wild-type protein. All effects on key mediators (PGE<sub>2</sub> and IL-10) (Fig. 5D and fig. S7E) or target genes (Fig. 5E) induced by heGDH were lost in the absence of the N terminus (residues 1 to 33), even when cells were stimulated with a higher dose (fig. S7F). In contrast, heGDH<sup>C136S</sup> showed similar activity to the wild-type protein, identifying the N terminus as the key feature responsible for specific effects of heGDH.

## heGDH interacts with proteins involved in macrophage activation and antihelminth immunity, including CD64

To identify cellular targets of heGDH, human MDMs were stimulated with hemagglutinin (HA)-tagged heGDH (HA-heGDH) for 30 min or 24 hours. In one set of experiments, HA-heGDH was again added into the lysate before immunoprecipitation (IP) using anti-HA or isotype control beads. Proteomic analysis revealed 16 overlapping proteins between the two experiments for both time points (Fig. 5F and table S1). heGDH was identified as one of the most abundant proteins even when used only for stimulation and not added to the lysate, supporting efficient uptake into macrophages (Fig. 5G and table S1). Fc gamma receptor (CD64) and transmembrane glycoprotein NMB (GPNMB) were identified as the most abundantly bound proteins by heGDH (relative to isotype control) (Fig. 5, G and H, and table S1). Direct binding of HA-heGDH to CD64 was validated by co-IP of the purified proteins in vitro (fig. S7G). Thus, noncatalytical features of heGDH enable interactions with factors involved in type 2 immunity and antihelminth host defense [CD64 (35) and DGAT1 (36)] as well as with GPNMB, implicated in tissue repair and alternatively activated macrophage (AAM) activation (37, 38)). By binding to these targets, heGDH may enter the cell, interfere with antibody-dependent activation, and/or induce metabolic and epigenetic reprogramming (35, 39, 40).

## Suppression of LTs is mediated via metabolic reprogramming

Our data suggested that heGDH can regulate LTs, which may promote antihelminth immunity (14) via its catalytic activity. Thus, we next aimed to elucidate effects of heGDH on macrophage metabolism. In mammalian tissues, oxidative deamination of glutamate via GDH generates α-KG, which can fuel the TCA cycle and further generate adenosine triphosphate (ATP) in oxidative phosphorylation (OXPHOS). Metabolic flux analysis revealed that, in line with the suppressive capacity of heGDH on AAM activation, macrophage metabolism shifted toward increased basal glycolysis, typical for M1-activated macrophages (Fig. 6A and fig. S8A) (41). In contrast, AAMs have been shown to rely primarily on OXPHOS, which tended to be down-regulated by heGDH (Fig. 6A and fig. S8A). The significant p300- and H3K27ac-dependent up-regulation of the gene PFKFB3 (Fig. 6B), a positive regulator of glycolysis, after heGDH stimulation suggested a potential link between glycolysis and heGDH-induced epigenetic reprogramming (Fig. 6C and fig. S8B). Inhibition of p300 activity in MDMs during treatment with heGDH blocked the decrease in basal respiration and ATP production as well as the increase in basal glycolysis (Fig. 6D), suggesting that the metabolic shift triggered by heGDH is p300 dependent. LC-MS/MS analysis of TCA metabolites revealed higher levels of 2-hydroxyglutarate (2-HG) in heGDH-treated MDMs, whereas the

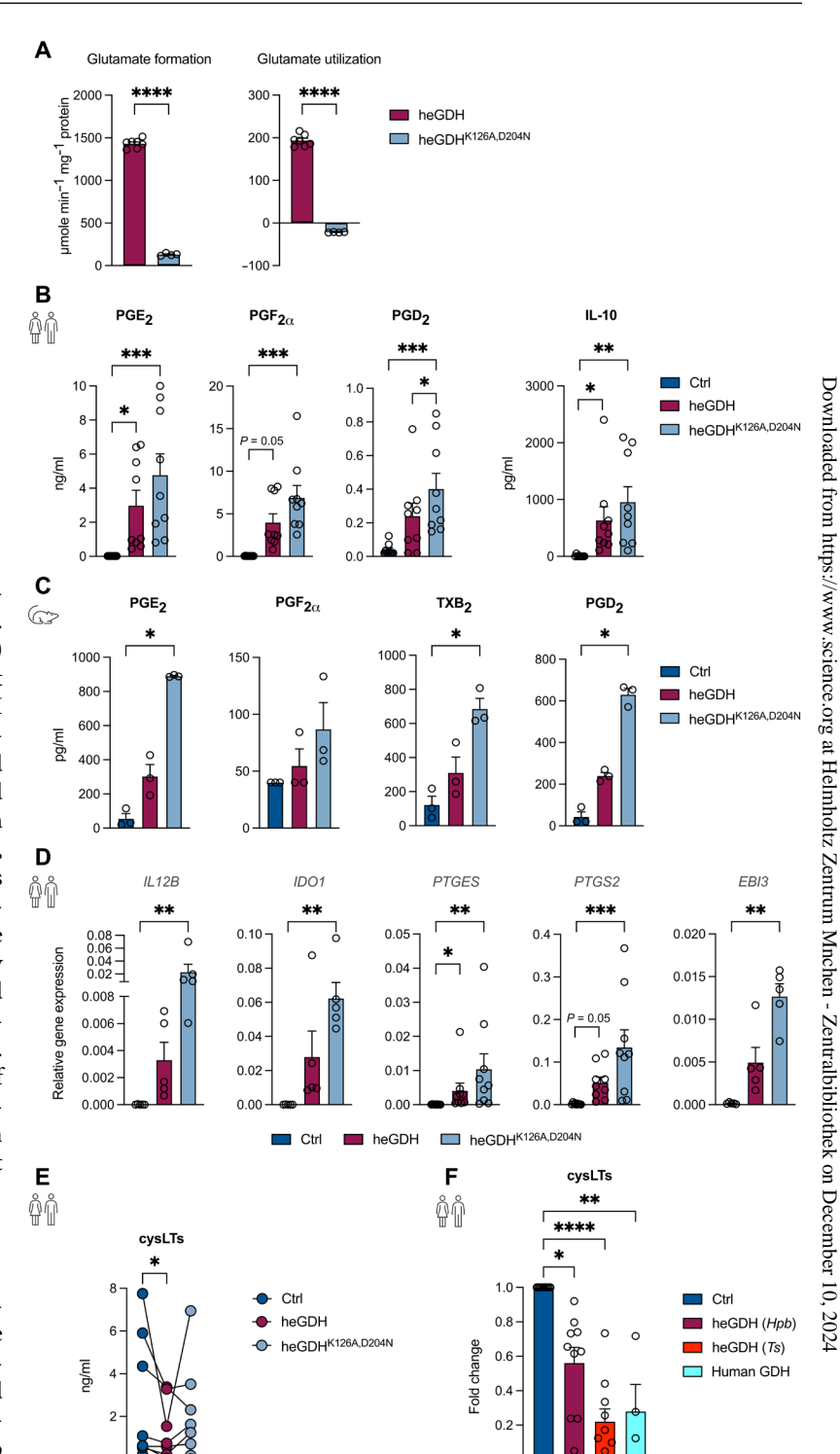
Fig. 4. Noncatalytic features of heGDH confer its major immune regulatory functions. (A) GDH activity of heGDH and heGDH<sup>K126A, D204N</sup> in the direction of glutamate utilization and formation (n = 7replicates for heGDH, n = 4 replicates for heGDH<sup>K126A, D204N</sup>). (**B**) Levels of prostanoids (LC-MS/MS) and IL-10 (ELISA) produced by MDMs  $\pm$ heGDH (5  $\mu$ g/ml) or heGDH<sup>K126A, D204N</sup> (n = 9 donors). (**C**) Levels of major COX metabolites (LC-MS/MS) produced by BMDMs ± heGDH (5  $\mu$ g/ml) or heGDH<sup>K126A, D204N</sup> (n = 3 mice). (**D**) Gene expression analysis of top DEGs (qPCR) in MDMs  $\pm$  heGDH (5  $\mu$ g/ml) or heGDH<sup>K126A, D204N</sup> (n = 5 donors for IL12B, IDO1, and EBI3; n = 9 donors for PTGES and PTGS2). (E) Secretion of cysLTs (EIA) from MDMs  $\pm$  heGDH (5  $\mu$ g/ ml) or heGDH<sup>K126A, D204N</sup> (n = 8 donors). (**F**) FC of cysLT secretion (EIA) from MDMs  $\pm$  heGDH (5  $\mu$ g/ml; *Hpb* or *Ts*) or human GDH (n =4 donors for human GDH, n = 10 donors for heGDHs). Data are pooled from at least two independent experiments and presented as means + SEM. Statistical significance was determined by unpaired t test (A), Friedman test [(B) to (E)], or Kruskal-Wallis test (F). \*P < 0.05, \*\*P < 0.01, \*\*\*P < 0.001, and \*\*\*\*P < 0.0001.

levels of glutamine and glutamate were reduced compared with those in untreated MDMs (Fig. 6, E and F). Furthermore, the aconitate decarboxylase 1 (*ACOD1*) product itaconate, an immunoregulatory by-product of the TCA cycle, was increased in response to heGDH (Fig. 6E). To determine whether the downstream metabolites of heGDH (itaconate, α-KG, and 2-HG) could affect immune regulatory AA metabolites, we assessed eicosanoid production by MDMs after treatment with these metabolites (fig. S8C). We observed that L-2-HG, but not D-2-HG, reduced the production of cysLTs (Fig. 6G and fig. S8D). To investigate whether L-2-HG directly affects the catalytic activity of leukotriene C<sub>4</sub> synthase (LTC4S), we performed an LTC4S activity assay. Although LTC4S activity was partially inhibited by addition of L-2-HG (Fig. 6H), gene expression levels of ALOX5 and LTC4S were not affected (fig. S8E). heGDH also directly affected the enzymatic activity of recombinant LTC4S (Fig. 6I) as well as in a human macrophage cell line (fig. S8F). Thus, effects of heGDH on the synthesis of key mediators of type 2 immunity are at least in part mediated by its downstream metabolites.

## heGDH-induced PGE<sub>2</sub> suppresses type 2 effector functions of macrophages and T cells

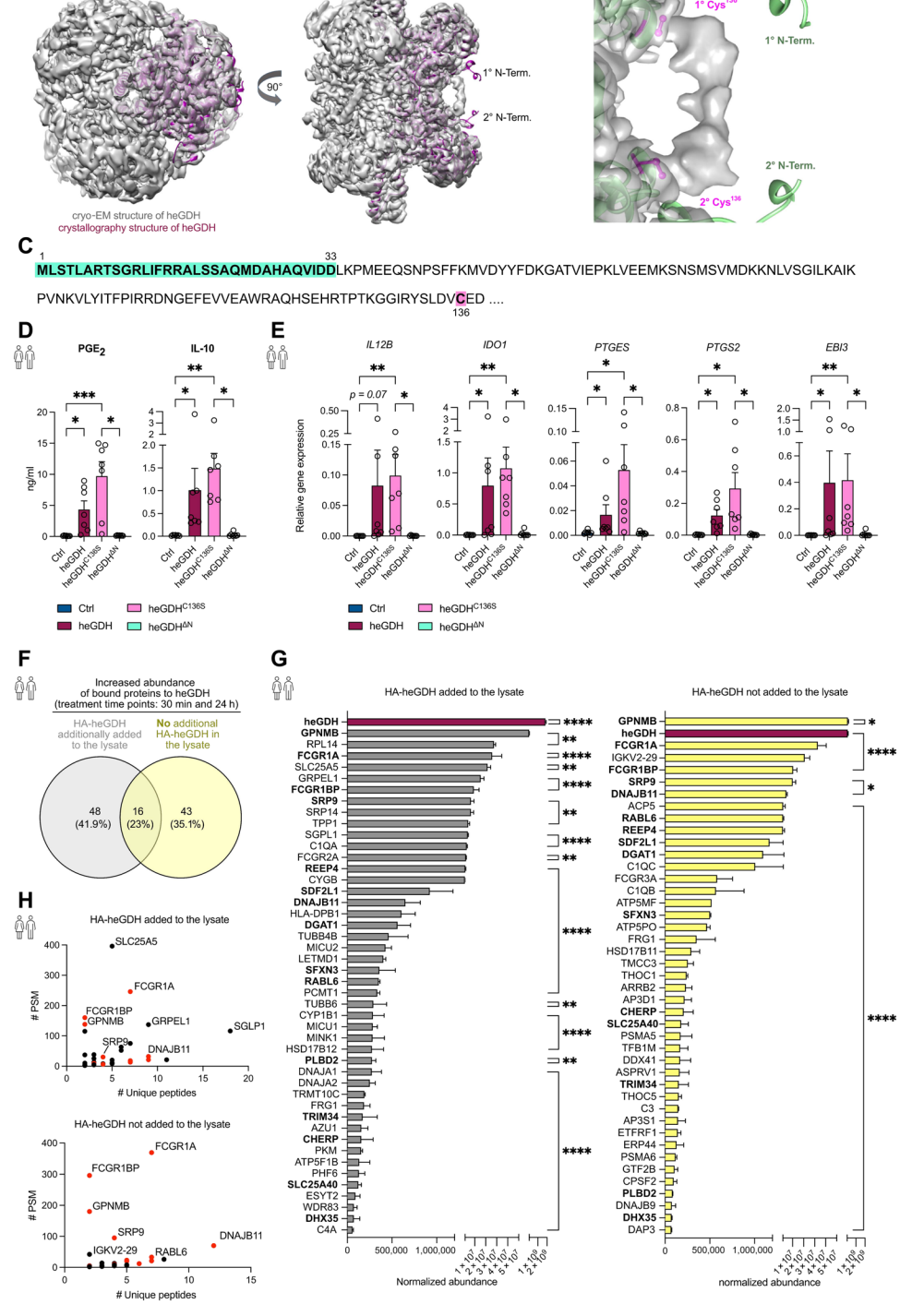
To investigate whether recombinant heGDH can modulate host defense in vivo, mice infected with *Hpb* were treated (intraperitoneally) with the heGDH protein during the tissue-dwelling phase of the parasite, associated with trapping and killing by AAMs (Fig. 7A). Our combined RNA-seq, ChIP-seq, and proteomic data (Figs. 1 to 6) suggested that heGDH suppresses multiple key steps in the activation of AAM effector functions essential for host

defense against parasitic nematodes (4, 5, 42). In keeping with these suppressive effects, administration of heGDH led to a significant increase in worm burdens at 14 days p.i. and reduced expression of the AAM markers resistin-like molecule  $\alpha$  (RELM $\alpha$ ) and the rodent-specific chitinase like proteins Ym-1/2, whereas the M1 marker inducible nitric oxide synthase (iNOS) was increased (Fig. 7, B and C, and fig. S9A). In line with our in vitro data (Fig. 3), peritoneal



macrophages from heGDH-treated mice showed increased H3K27ac, correlating with enhanced PGE<sub>2</sub> production and expression of COX-2 in the small intestine (Fig. 7, C to E, and fig. S9B). Reduced down-regulation of CD206 in heGDH-treated BMDMs from naïve mice lacking the PGE<sub>2</sub> receptor EP2 supported a key role for PGE<sub>2</sub> in the regulation of AAM activation (Fig. 7F). Assessment of heGDH's impact on helminth chronicity at a later time point (28 days p.i.) (Fig.

Fig. 5. heGDH interacts with multiple proteins involved in macrophage activation and induces immune regulatory mediators via its N terminus. (A) Model of the heGDH crystal structure fitted in the oligomeric cryo-EM reconstruction. N termini of two neighboring subunits, which are resolved in the x-ray structure, are near to a handlelike density in the cryo-EM model. (B) Close-up of the handle-like density and the N termini from the heGDH crystal structure fitted in the cryo-EM reconstruction. (C) N-terminal part of the heGDH sequence highlighting the N terminus in green and essential amino acid C136 for forming the handlelike density in pink. (D) Secretion of PGE<sub>2</sub> and IL-10 (EIA and ELISA) from MDMs  $\pm$  heGDH (5  $\mu g/ml),$ heGDH<sup>C136S</sup>, or heGDH<sup> $\Delta N$ </sup> (n = 7 donors). (**E**) Gene expression analysis of top DEGs (qPCR) in MDMs  $\pm$ heGDH (5  $\mu$ g/ml), heGDH<sup>C136S</sup>, or heGDH<sup> $\Delta$ N</sup> (n=7donors). (F) Venn diagram comparing two independent experiments (5 µg of HA-heGDH added to the MDM lysate versus not added to the MDM lysate before IP) for two time points [30 min and 24 hours (h)] to identify the overlapping proteins binding to heGDH. (G) Normalized abundance of bound proteins to HA-heGDH for both time points (30 min and 24 hours). Left: Five micrograms of HAheGDH was additionally added to the MDM lysate. Right: HA-heGDH was not additionally added. Proteins marked bold represent the overlap of binding to HA-heGDH between both experiments. (H) Identified proteins [proteomics, peptide spectrum matches (PSMs) versus unique peptides] binding to HAheGDH from two different experiments. Top: with addition of 5  $\mu g$  of HA-heGDH to the MDM lysate. Bottom: without addition of HA-heGDH to the MDM lysate. Red dots represent overlapping proteins identified in both experiments. Data are pooled from at least two independent experiments and presented as means + SEM. Statistical significance was determined by Friedman test [(D) and (E)] or background-based t test (G). \*P < 0.05, \*\*P < 0.01,\*\*\*P < 0.001, and \*\*\*\*P < 0.0001.

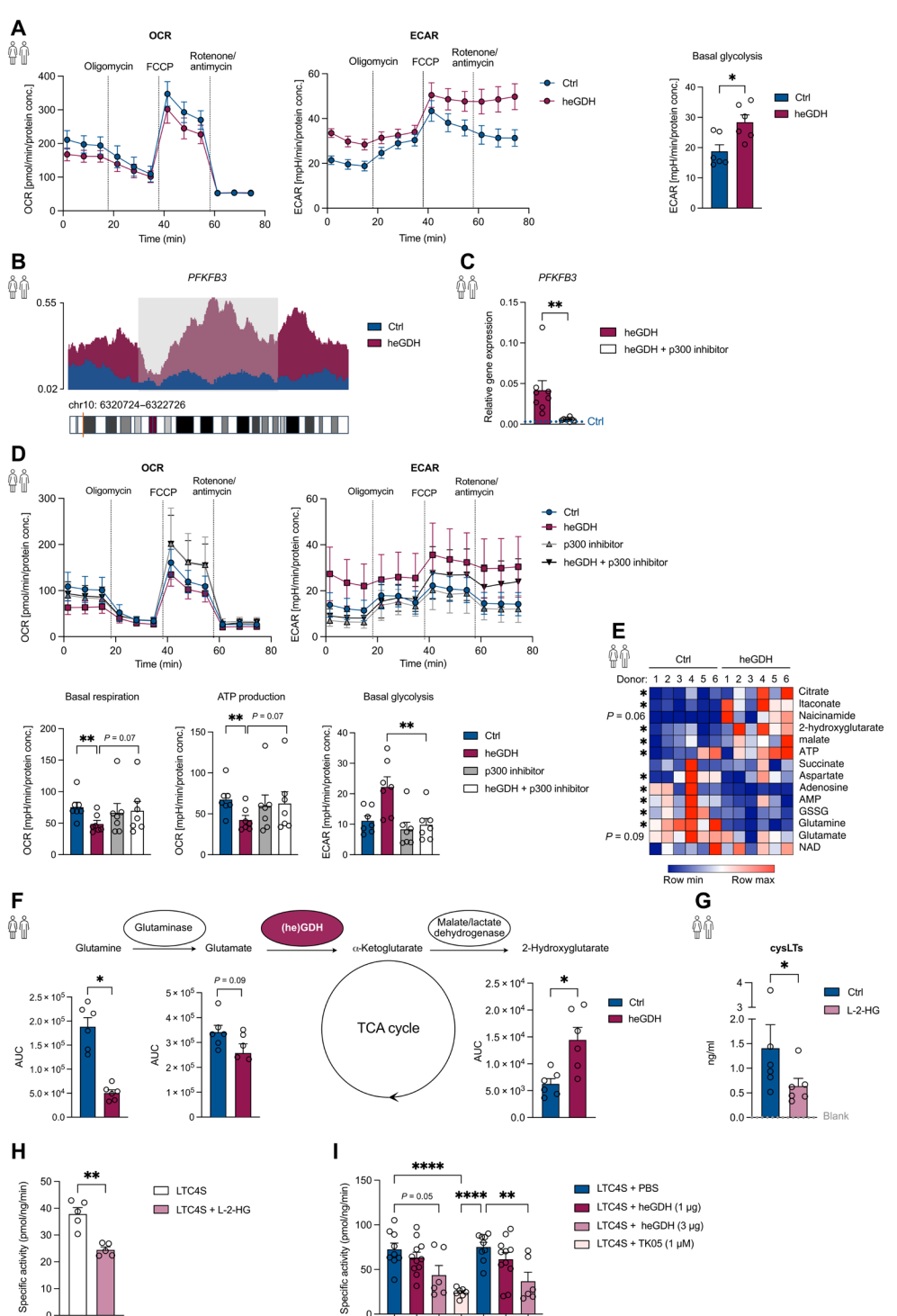


В

7G) yielded an even stronger increase in worm burdens compared with day 14 (Fig. 7, B and H) and tended to increase egg counts (fig. S9C), supporting the role of heGDH in promoting helminth chronicity (Fig. 1B). Although treatment with heGDH did not induce PGE<sub>2</sub> in peritoneal macrophages (Fig. 7I) at this later time point, other prostanoids (TXB<sub>2</sub> and 6-keto-PGF<sub>1 $\alpha$ </sub>) associated with tissue repair (29) were increased in the small intestines of mice treated with

heGDH (Fig. 7J). However, parameters of intestinal tissue repair [myofibroblast and  $\alpha$ -smooth muscle actin ( $\alpha$ -SMA) accumulation and collagen deposition] (22) remained unaffected by heGDH (fig. S9, D to F). heGDH treatment also reduced the percentage of Gata3<sup>+</sup>  $T_{\rm H}2$  cells and type 2 cytokine expression in the mesenteric lymph nodes (MLNs) at 28 days after Hpb infection, whereas  $T_{\rm H}2$  activation was unaffected at earlier time points (Fig. 7K and fig. S9, G to I).

Fig. 6. Suppression of LTs is mediated via metabolic reprogramming. (A) Oxygen consumption rate (OCR, left), extracellular acidification rate (ECAR, middle), and basal glycolysis (right) with injections of 1 μM oligomycin, 1 μM FCCP, and 0.5  $\mu$ M rotenone/antimycin of MDMs  $\pm$  heGDH treatment (5  $\mu$ g/ml; n = 6 donors). (**B**) H3K27ac ChIP-seq signal of MDMs  $\pm$  heGDH (5  $\mu$ g/ml; n =3 donors) for the PFKFB3 peak (gray window; FDR  $\leq$  0.05; absolute  $\log_2$  FC > 1). (**C**) Gene expression analysis of PFKFB3 (qPCR) in MDMs + heGDH  $(5 \mu g/ml) \pm 6.6 \mu M p300 HAT inhibitor (A485) (n =$ 8 donors). Dotted line indicates expression in control (Ctrl) cells. (D) Top: OCR and ECAR with injections of 1  $\mu$ M oligomycin, 1  $\mu$ M FCCP, and  $0.5 \mu M$  rotenone/antimycin A of MDMs  $\pm$  heGDH  $(5 \mu g/ml) \pm 6.6 \mu M p300 HAT inhibitor (A485).$ Bottom: Basal respiration, ATP production, and basal glycolysis of MDMs  $\pm$  heGDH (5  $\mu$ g/ml)  $\pm$ 6.6  $\mu$ M p300 HAT inhibitor (A485) (n=6 donors for OCR and ECAR; n = 7 donors for basal respiration, ATP production, and basal glycolysis). (E) Heatmap of targeted metabolomics (LC-MS/MS) in MDMs  $\pm$  heGDH (5  $\mu$ g/ml; n = 6 donors). AMP, adenosine monophosphate; GSSG, oxidized glutathione. (F) Targeted metabolomics (LC-MS/MS) for glutamine, glutamate, and 2-HG in MDMs  $\pm$ heGDH (5  $\mu$ g/ml; n = 6 donors). AUC, area under the curve. (G) Secretion of cysLTs (EIA) by MDMs  $\pm$  1 mM L-2-HG (n=6 donors). (**H**) LTC4S activity after incubation with 1 mM L-2-HG (n = 5 replicates). (I) LTC4S activity after addition of heGDH (1 or 3  $\mu$ g) or a specific LTC4S inhibitor (1  $\mu$ M, TK05) (n = 6 to 11 replicates). Data are pooled from at least two independent experiments and presented as means + SEM. Statistical significance was determined by Wilcoxon test [(A), (C), and (E) to (G)], Mann-Whitney test (H), Friedman test (D), or ordinary one-way ANOVA (I). \*P < 0.05, \*\*P < 0.01, and \*\*\*\*P < 0.0001.



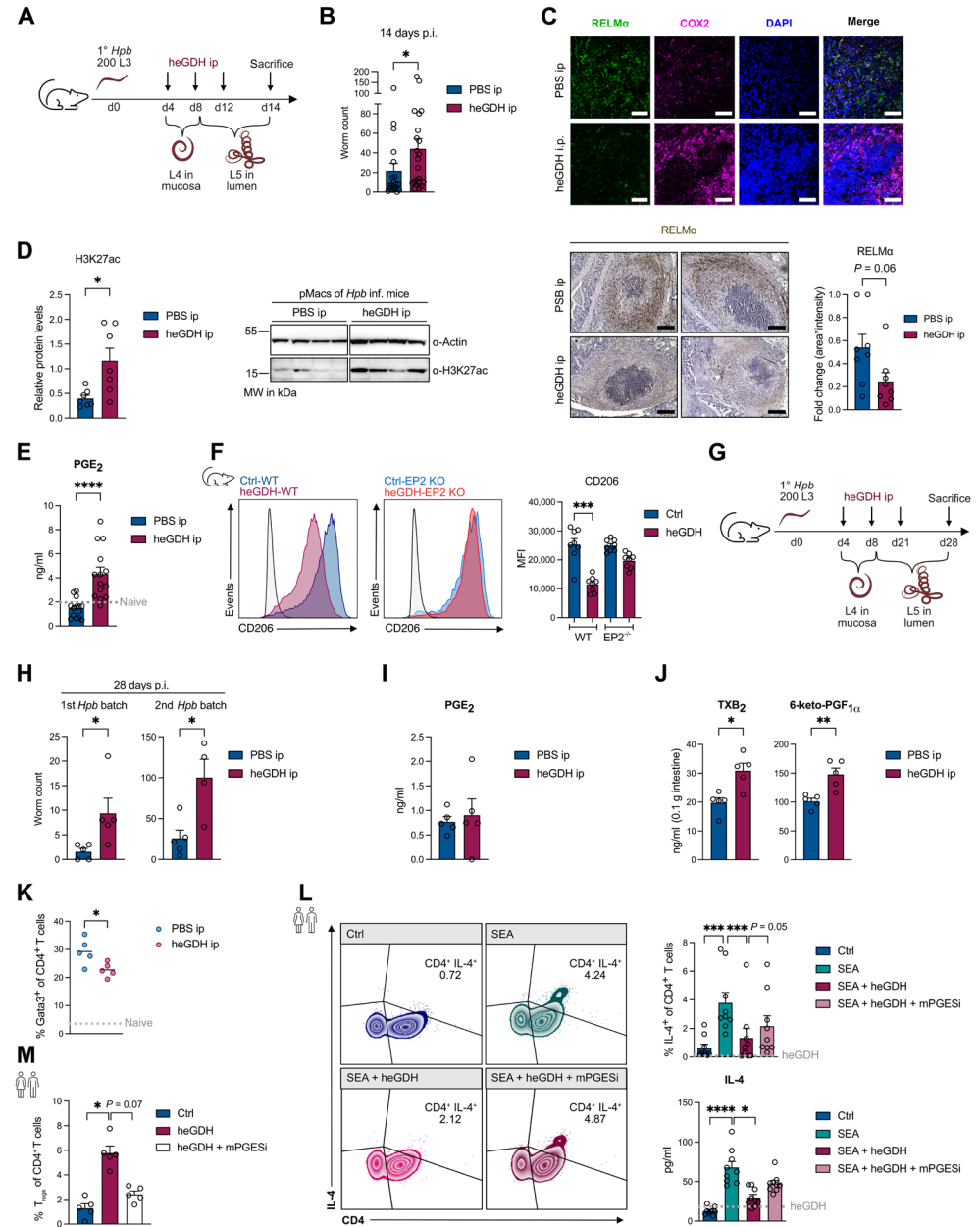
To investigate the importance of heGDH-triggered  $PGE_2$  in the regulation of helminth-induced  $T_{H2}$  responses, we analyzed the capacity of heGDH to reduce type 2 cytokine production in human peripheral blood mononuclear cells (PBMCs) after stimulation with *Schistosoma mansoni* soluble egg antigen (SEA), a strong parasitic  $T_{H2}$  trigger. The percentage of SEA-induced IL-4<sup>+</sup>CD4<sup>+</sup>  $T_{H2}$  cells was significantly reduced, and SEA-induced IL-4 production was

diminished after heGDH treatment (Fig. 7L), whereas heGDH induced CD4 $^+$ CD127 $^-$ CD25 $^{hi}$ FoxP3 $^+$  T<sub>regs</sub> in human PBMCs (Fig. 7M). These T cell modulatory functions of heGDH were abrogated by a selective inhibitor of mPGES-1 (Fig. 7, L and M) or depletion of monocytes (fig. S9J), indicating that PGE<sub>2</sub> acts as a key modulator of macrophage and T cell function during heGDH-induced helminth chronicity.

5  $\mu$ g of heGDH (n=5 mice per group). Dotted line indicates percentage in MLNs from naïve mice. (**L**) Percentage of IL-4<sup>+</sup> T<sub>H</sub>2 cells (flow cy-

Fig. 7. heGDH-induced PGE<sub>2</sub> suppresses type

2 effector functions of macrophages and T



tometry) and secretion of IL-4 (ELISA) from human PBMCs  $\pm$  SEA (50  $\mu$ g/ml)  $\pm$  heGDH (5  $\mu$ g/ml)  $\pm$  10  $\mu$ M mPGES1 inhibitor (934) (n=9 donors). (M) Percentage of CD4+CD127-CD25<sup>hi</sup>FoxP3+ (flow cytometry) in human PBMCs  $\pm$  heGDH (5  $\mu$ g/ml)  $\pm$  10  $\mu$ M mPGES1 inhibitor (934) (n=5 donors). Data are pooled from two to five independent experiments and presented as means + SEM. Statistical significance was determined by Mann-Whitney test [(B) to (E) and (H) to (K)], Kruskal-Wallis test (F), or Friedman test [(L) and (M)]. \*P < 0.05, \*\*P < 0.01, \*\*P < 0.01, \*\*P < 0.001, and \*\*\*P < 0.001, intraperitoneally.

## Host type 2 immunity limits immune evasion but not tissue repair driven by heGDH

To assess how host type 2 immunity may affect heGDH-driven immune regulation, we mimicked a type 2 milieu in vitro by culturing MDMs and BMDMs in the presence of IL-4 and IL-13 before treatment with heGDH. IL-4/IL-13-induced genes (*ALOX15* and *MRC1* in human MDMs; *Retnla*, *Chil3*, and *Mrc1* in murine BMDMs) were or tended to be down-regulated by heGDH, confirming the prevention of AAM polarization in a type 2 cytokine milieu (Fig. 8A and fig. S10A). Although some heGDH-induced genes, including *IDO1*,

*IL12B*, and *EBI3*, were unaffected by additional treatment with IL-4 and IL-13 (Fig. 8B and fig. S10A), IL-4 and IL-13 suppressed the induction of *PTGS2* and *PTGES* as well as PGE<sub>2</sub> (Fig. 8, C and D). In line with these counterregulatory effects of type 2 cytokines, the capacity of heGDH to trigger immune evasion was impaired during strong type 2 immune responses, i.e., during challenge infection with *Hpb* or infection with *Nippostrongylus brasiliensis* (*Nb*) (Fig. 8, E, F, I, and J). However, treatment (intraperitoneal) with heGDH still resulted in a tendency toward increased worm burdens (Fig. 8F) and a significant reduction of the AAM markers RELMα and Ym-1/2 during

challenge infection with Hpb (Fig. 8G and fig. S10B). To study whether heGDH may directly affect macrophage-mediated trapping of Hpb larvae (5), immune serum-activated macrophages were coincubated with L3 in the presence or absence of heGDH. Macrophagemediated larval trapping was impaired by heGDH (movie S1), showing that heGDH directly suppresses a key macrophage effector function during helminth infection. As during primary infection, heGDH treatment did not affect T cell composition or levels of arginase 1 (Arg1), α-SMA, or collagen in the small intestine during challenge infection (figs. S9B and S10, C to F), suggesting that tissue repair remained unaltered. In line with blunted prostanoid induction and immune evasion in the presence of type 2 cytokines (Fig. 8, C and F), PGE<sub>2</sub> secretion by peritoneal macrophages and up-regulation of COX-2 by heGDH were attenuated in the granulomas of challenge-infected as compared with primaryinfected mice (Figs. 7, C and E; Figs. 8, G and H; and fig. S10D). Intranasal treatment with heGDH during infection with Nb (Fig. 8I), a helminth that triggers a rapid type 2 immune response, similarly failed to significantly affect intestinal worm burdens (Fig. 8J). Despite increasing airway neutrophils and IL-6 and IL-17A production, intranasal heGDH treatment reduced leukotriene B<sub>4</sub> (LTB<sub>4</sub>) synthesis, collagen deposition, and lung damage in Nb-infected mice (Fig. 8, L and M, and fig. S11, A to C). Intestinal eicosanoid profiles as well as T cell responses in the lung and MLN remained largely unaffected by intranasal heGDH treatment except for PGE2, which was increased in the intestines of naïve mice (fig. S11, D to F), suggesting that heG-DH can influence the lung-gut axis. The decreased type 2 immune response and improved tissue repair in mice treated with heGDH during Nb infection correlated with an increase in antifibrotic factors (Arg1 and PGE2) (43, 44) in bronchoalveolar lavage (BAL) macrophages (Fig. 8K and fig. S11G). Together, this suggests that type 2 immune responses have evolved to overcome helminth/GDH-driven immune evasion while leaving tissue reparative and proresolving functions of immune regulatory helminth molecules intact.

## **DISCUSSION**

The present study identifies key roles of heGDH in immune evasion, parasite chronicity, and tissue repair during helminth infections, which represent a major global health burden (45). heGDH targets host macrophages, resulting in metabolic, epigenetic, and transcriptional changes that broadly suppress antihelminth effector functions. Catalytic activity and noncatalytical features of heGDH synergize to suppress mediators of type 2 immunity and induce factors that regulate macrophage and T cell activation. Macrophages play crucial roles in antihelminth immunity by trapping worms, regulating T cell responses, and repairing tissue damage (5, 7, 8, 12, 18, 29), making them prime targets of parasitic immune evasion (21). CD64-positive macrophages colocalize with GDH-containing helminth larvae in the small intestine, and our proteomic analysis identified CD64 and GPNMB as potential targets of heGDH. The antibody-driven activation of macrophages via CD64 plays an important role in helminth trapping (8, 35), suggesting that heGDH binds CD64 to ensure efficient uptake and evade macrophage-mediated immunity. Although we do not provide experimental evidence that directly links CD64 or GPNMB to p300 activation, a previous study demonstrated that C-reactive protein can bind CD64, resulting in hypoxiainducible factor  $1\alpha/p300$ -dependent transcriptional activation (46). Furthermore, GPNMB up-regulates H3K27 lysine demethylase Jumonji domain-containing protein-3 (JMJD3) (40), which cooperates with p300 to switch toward H3K27ac-mediated transcriptional activation (47). This suggests that heGDH targets multiple factors involved in epigenetic reprogramming and AAM activation to efficiently interfere with antihelminth immunity (37). Given that helminth infections often occur in early life, GDH-driven epigenetic reprogramming of macrophages and their progenitors in the bone marrow may have long-lasting effects on subsequent immunity to infections that need further investigation. Down-regulation of key factors involved in myelopoiesis (MYB and MYBL2) by heGDH suggests the modulation of central trained immunity. In contrast to the suppression of several key IL-4/IL-13-induced genes (Mrc1/ CD206, Alox15, Chil3/ Ym1, and Fizz1/ RELMα) by heGDH, the enzyme does not target Arg1, suggesting that Arg1-mediated regulation of T<sub>H</sub>2 responses (43) remains intact in the presence of heGDH.

Although heGDH triggers a broad epigenetic and transcriptional reprogramming, our data support a key role for PGE<sub>2</sub> in GDH-driven helminth chronicity. heGDH-induced PGE<sub>2</sub> suppresses AAM polarization and T<sub>H</sub>2 cell activation, two essential mechanisms of antihelminth immunity (4, 7, 42). In addition, PGE<sub>2</sub> may limit type 2 innate lymphoid cell (ILC2) and mast cell function (45, 48, 49), suggesting that heGDH affects multiple cell types involved in type 2 immunity. It will be important to investigate whether heGDH targets additional cell types involved in the initiation of type 2 immunity, including tuft cells, a major early source of host-protective cysLTs (14). Given the roles of eicosanoids in tissue repair (50-53), it will be interesting to investigate whether prostanoids are responsible for tissue-reparative effects of heGDH, e.g., using mice with deficiencies in PGE2 synthesis (54). In contrast to heGDHs, human GDH fails to trigger the PGE2-dependent induction of Tregs (18), suggesting that the N terminus, which is distinct from mammalian GDHs, allows for interactions of heGDH with its targets (e.g., CD64 and GPMNB), thus conferring specific immune regulatory effects to heGDH. An N-terminal truncation mutant of heGDH showed a complete loss of all tested immune regulatory effects (including the induction of PGE<sub>2</sub> and IL-10), suggesting that the exposed N termini in the heGDH hexamer provide key docking sites for interaction partners.

Although the induction of type 2-suppressive factors [PGE<sub>2</sub>, indoleamine 2,3-dioxygenase 1 (IDO1), and IL-12 family cytokines]) shared the same structure and p300-dependent upstream mechanism, the suppression of type 2-promoting cysLTs depended on the catalytic activity of GDH. L-2-HG induced by heGDH can interfere with LTC4S activity to reduce the synthesis of cysLTs, important for early antihelminth immunity (14). However, the precise mechanism by which L-2-HG limits LTC4S activity remains to be determined. Given that LTC4S activity is controlled by phosphorylation via the mammalian target of rapamycin (mTOR)/p70S6K pathway (55, 56), which is activated by 2-HG (57), it would be interesting to assess whether heGDH triggers inhibitory phosphorylation of LTC4S. Although our data suggest that heGDH can be taken up by macrophages, whether this uptake is required for immune regulation remains unclear. Moreover, our study does not clarify whether and how heGDH is released from the parasite and how this may result in the preferential targeting of macrophages. Given that Heligmosomoides polygyrus only infects mice, the findings from the current study may not be directly translatable to human helminth infection.

Despite these limitations, a conserved role of GDHs in parasite chronicity is supported by studies identifying GDH as a dominant

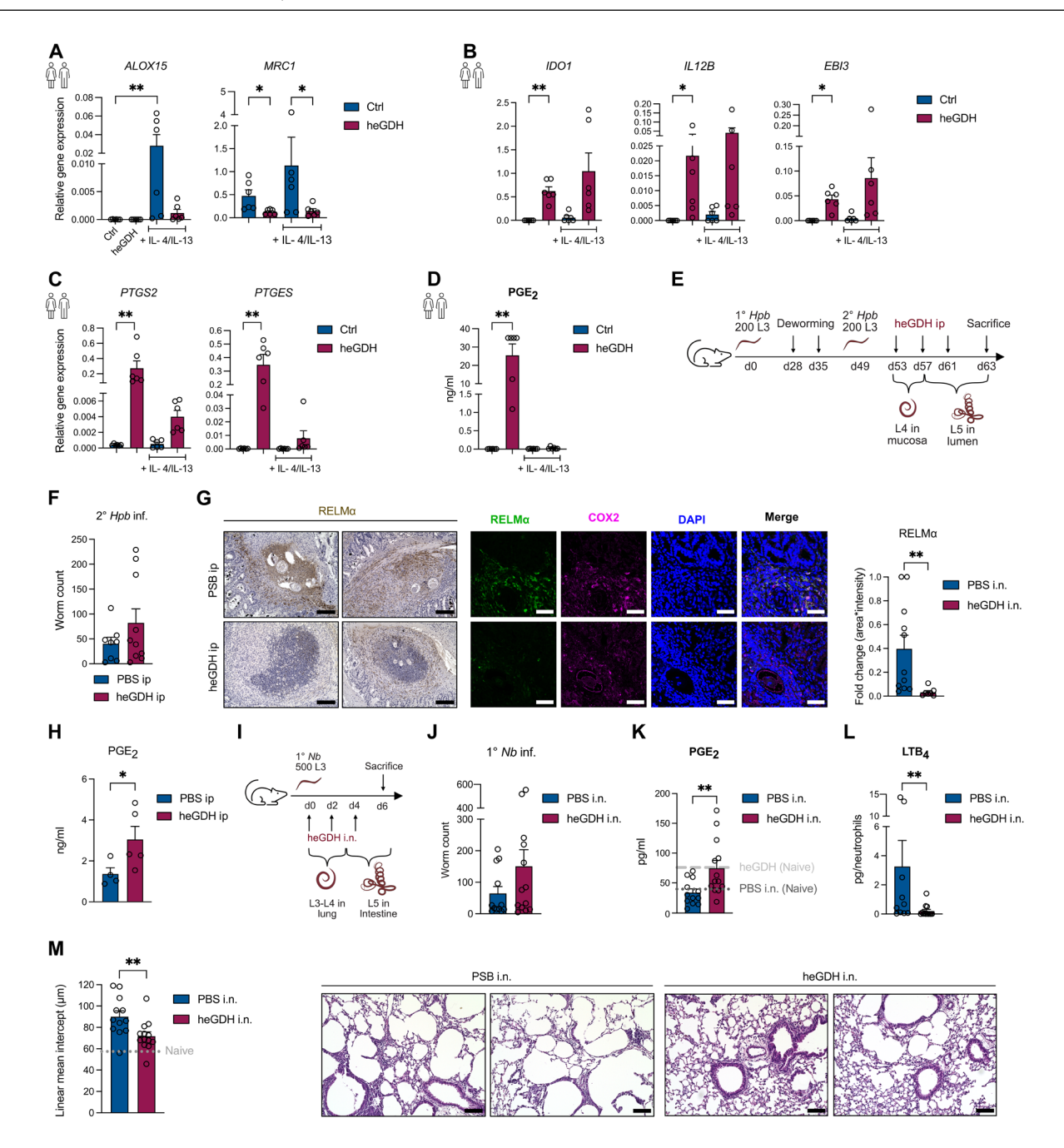


Fig. 8. Host type 2 immunity limits immune evasion but not tissue repair driven by heGDH. (A to C) Gene expression analysis of AAM markers (A), top DEGs (B), or PGE<sub>2</sub> synthesis genes (C) (qPCR) in human MDMs  $\pm$  heGDH (5 μg/ml) or after IL-4 and IL-13 (20 ng/ml) pretreatment (n = 6 donors). (E) Experimental model of secondary Hpb infection and heGDH treatment. (F) Worm burdens 14 days after secondary Hpb infection in mice treated with PBS or 5 μg of heGDH (n = 8 mice in the PBS group; n = 10 mice in the heGDH group). (G) Left: Representative images of IHC staining for RELMα. Scale bars, 150 μm. Middle: Representative images of IF staining for RELMα (green), COX2 (magenta), and DAPI (blue). Scale bars, 50 μm. Right: Quantification of RELMα in granulomas of tissues from challenge Hpb-infected mice treated with PBS or 5 μg of heGDH (n = 11 mice in the PBS group; n = 7 mice in the heGDH group). (H) Secretion of PGE<sub>2</sub> (EIA) by pMacs (14 days post–challenge infection) of mice treated with PBS or 5 μg of heGDH (n = 5 mice per group). (I) Experimental model of Nb infection treated intranasally (i.n.) with PBS or 10 μg heGDH. (J) Nb worm burdens 6 days p.i. in mice treated with PBS or 10 μg of heGDH (n = 12 mice in the PBS group; n = 13 mice in the heGDH group). (K) Secretion of PGE<sub>2</sub> (EIA) by BAL macrophages from Nb-infected mice treated with PBS or 10 μg of heGDH (n = 12 mice in the PBS group; n = 13 mice in the heGDH group). Dotted line indicates secretion from BAL macrophages of naïve mice treated with PBS or 10 μg of heGDH (n = 12 mice in the PBS group; n = 13 mice in the heGDH group). (M) Left: Quantification of lung damage as Lmi (n = 12 mice in the PBS group; n = 13 mice in the heGDH group). Right: Representative hematoxylin and eosin stainings of lung sections from Nb-infected mice treated with PBS or 10 μg of heGDH (n = 10 mice in dicates Lmi of naïve mice. Data are pooled from two to four independent experiments and presented as means + SEM. Statistical signifi

vaccine target (58) and showing immunomodulatory effects of GDH from the protozoan parasite *Trypanosoma cruzi* as well as from the parasitic cestode *Ts* (18, 59). Future research should thus determine whether GDHs from different parasites use the same mechanisms to drive chronicity and tissue repair. The weakened effects of heGDH in the presence of a full-blown type 2 immune response suggest that host type 2 immunity has evolved to counteract helminth-driven immune regulation. The present study thus identifies an important pathway of host-parasite cross-talk via a ubiquitous metabolic enzyme, which may be harnessed for the therapy or prevention of major infectious and inflammatory diseases.

### **MATERIALS AND METHODS**

## Study design

The aim of this study was to investigate how GDH derived from *Hpb* can modulate eicosanoid pathways and macrophage activation to regulate the host type 2 immune response. To accomplish this, we used transcriptomic and epigenetic analysis (RNA-seq and ChIP-seq), qPCR, LC-MS/MS, and enzyme-linked immunosorbent assay (ELISA). To define in vivo effects of heGDH, mice were treated with an mAb against heGDH or with recombinant heGDH during parasite infections. Effects of heGDH or clone 4F8 treatment on worm counts, histology, and prostaglandin production in host macrophages were assessed during infection with *Hpb* or *Nb* in vivo. To investigate the involvement of metabolism on eicosanoid production by heGDH, metabolic changes in macrophages were determined by targeted metabolomics and seahorse assays. To untangle the role of structure versus catalytic function of heGDH, a catalytically inactive mutant, a mutant lacking the handle-like density (C136S), and a mutant lacking the N terminus were produced recombinantly; the structure of heGDH was elucidated; and proteomic analysis of heGDH-treated human macrophages was performed. For the human part of our study, healthy volunteers (total n = 53) (Caucasian men and women) were recruited. Sample sizes (determined by power analysis by a statistician), replicates, and statistical methods are specified in the figure legends. All blood donors participated in the study after informed written consent. All procedures were approved by the local ethics committee at the University clinic of the Technical University of Munich (internal reference: 802/20S) and in accordance with the Declaration of Helsinki.

### Mice

C57BL/6J mice were obtained from Charles River Laboratories (Sulzfeld) and maintained under specific pathogen–free conditions at the Helmholtz Munich or at the University of Lausanne. Unless stated otherwise, 6- to 12-week-old mice of both sexes were used. All animal experiments were approved by the local authorities (Regierung von Oberbayern, ROB-55.2-2532.Vet\_02-18-95 and canton de Vaud, VD3809c).

## Helminth infection, treatment with heGDH or mAb (clone 4F8), and parasitology readouts

Eight-week-old female mice were infected with Hpb by oral gavage with 100 or 200 L3 stage larvae diluted in 200  $\mu$ l of sterile PBS. Control animals received the same amount of PBS. Mice were euthanized at the indicated time points (14 or 28 days after primary or 14 days after secondary Hpb infection). heGDH treatment (5  $\mu$ g of heGDH in 100  $\mu$ l of PBS) was performed intraperitoneally at days 4, 8, and

12 for the 14-day primary infection experiment. When mice were euthanized at 28 days after primary infection, mice were treated at days 4, 8, and 21. Feces of 14- and 28-day primary-infected mice were collected at days 12, 14, 21, and 28 to quantify *Hpb* fecundity: Feces were weighed for normalization, and 500 µl of saturated sodium chloride solution was added. Feces was homogenized by vortexing. Suspensions were incubated at room temperature (RT) for 24 hours. The top layer was removed, and eggs were counted by a blinded experimenter. For secondary challenge infection, mice were infected with 200 Hpb larvae, and two courses of antihelminthic pyrantel (250 µg in 200 µl, intragastrically) were administered at days 28 and 35 p.i. Mice were reinfected with 200 larvae at day 49. Challengeinfected *Hpb* mice were treated with heGDH at days 53, 57, and 61. For blocking experiments, 10 μg of α-heGDH mAb (clone 4F8) or isotype control antibody (BioCell) in 100 µl of PBS was intraperitoneally given on days 0 to 2, 4, and 6. For Nb infection, mice were infected subcutaneously with 500 infectious third-stage larvae (L3). Control animals received the same amount of PBS. Intranasal treatment of Nb-infected mice with heGDH (10 μg of heGDH in 20 μl of PBS) was performed at days 0, 2, and 4. In the absence of heGDH treatment, mice received 100 µl of PBS intraperitoneally or 20 µl of PBS intranasally. Six days after Nb infection, BAL was performed five times with 0.8 ml of PBS. Aliquots of cell-free BAL fluid (BALF) were frozen immediately with or without equal volumes of methanol (MeOH) for LC-MS/MS and cytokine analysis. Viability, yield, and differential cell count of BAL cells were performed as previously described (60). The small intestines of Hpb- or Nb-infected mice were removed and opened to count adult worms (blinded experimenter) at the luminal surface using a light microscope. Analysis was performed on small intestinal tissues, MLNs, lung tissues, BAL samples, and peritoneal macrophages.

## Intestinal tissue culture

One to 2 cm of the small intestine was freed from mucus, extensively washed with cold PBS containing antibiotics (200 U/ml), and placed in 24-well plates with RPMI (1 ml per well) supplemented with antibiotics (200 U/ml). Tissue was incubated overnight (*Hpb*) or 6 hours (*Nb*) at 37°C before supernatants were harvested and analyzed by LC-MS/MS. Eicosanoid concentrations were normalized against tissue weight.

## **LEGENDplex** assay

The BALF supernatant from *Nb*-infected mice was analyzed by Multiplex cytokine assays [LEGENDplex MU Th Cytokine Panel (12-plex) w/ VbP V03, BioLegend] for the detection of murine interferon-γ, IL-5, tumor necrosis factor–α, IL-2, IL-6, IL-4, IL-10, IL-9, IL-17A, IL17F, IL-22, and IL-13. The kit was performed according to the manufacturer's instructions on a Accuri Flow Cytometer (BD Biosciences).

## **Culture and stimulation of MDMs or BMDMs**

CD14<sup>+</sup> PBMCs were used to generate MDMs as described previously (12). Macrophages were cultured in the presence of human granulocytemacrophage colony-stimulating factor (GM-CSF; 10 ng/ml; Miltenyi Biotec) and human transforming growth factor– $\beta$  (TGF- $\beta$ ; 2 ng/ml; PeproTech). BMDMs from bone marrow of wild-type C57BL/6 or EP2 $^{-/-}$  mice were isolated and cultured for 6 days in the presence of murine recombinant macrophage colony-stimulating factor (20 ng/ml; Miltenyi Biotech). Exchange of medium and replenishment of cytokines were performed on the third day. After 6 days, cells were harvested and used for stimulation experiments. When indicated, cells were treated for

24 hours with heGDH (5  $\mu g/ml)$ , same volume of mock vector purification, catalytically inactive heGDH  $^{K126A,\,D204N}$ , heGDH  $^{C136S}$ , heGDH  $^{\Delta N}$ , Ts GDH, or human GDH (Novus Biologicals). To analyze uptake of heGDH, macrophages were stimulated for 30 min, 3 hours, or 24 hours with Alexa Fluor 488-fluorochrome-labeled heGDH (5 µg/ml). To compare endotoxin-dependent effects, MDMs were stimulated with LPS (1 ng/ml; InvivoGen). For p300 inhibitor studies, 6.6 µM A485 (Tocris) was added 1 hour before heGDH stimulation. MDMs were harvested after 24 hours and BMDMs after 6 hours of stimulation with the p300 inhibitor. For experiments with neutralizing antibodies, MDMs were incubated with anti-heGDH mAb (clone 4F8) in a dilution of 1:100 prior heGDH stimulation. Stimulation of AAMs (MDMs and BMDMs) with heGDH was done after a 48-hour preincubation with human IL-4 and IL-13 (20 ng/ml; both from Miltenyi Biotec). Effects of TCA metabolites were assessed by stimulation of MDMs with 1 mM D-2-hydroxygluarate, L-2-HG, itaconate, or α-KG (all from Sigma-Aldrich, Merck) for 6 hours. Polyunsaturated fatty acid (PUFA) production was elicited by stimulating cells with 5 μM ionophore A23187 for 10 min at 37°C during harvesting. Cells were not treated with ionophore when they were used for fluorescence-activated cell sorting (FACS) analysis. Supernatants of cells were stored at -70°C in 50% MeOH for LC-MS/MS analysis or undiluted for cytokine analysis. Cell pellets were lysed in RLT buffer (Qiagen) with 1% β-mercaptoethanol (Merck Millipore) and stored at -70°C for RNA extraction. For protein immunoblot analysis, cell pellets were lysed with radioimmunoprecipitation assay (RIPA) buffer supplemented with complete protease inhibitor cocktail (Roche Applied Science) and stored at -70°C.

## Analysis of L3 Hpb trapping by BMDMs treated with heGDH

On day 6, BMDMs were harvested and stimulated for 24 hours with or without heGDH (5  $\mu$ g/ml). On the next day, cells were again treated with heGDH (5  $\mu$ g/ml) or control to block extracellular receptors. To all conditions, infective L3 stage *Hpb* larvae (1000 larvae/10<sup>6</sup> cells) and immune sera (1:50, v/v) were added. Serum samples were collected from challenge *Hpb*-infected mice on day 4 of secondary infection. All cocultures were performed at 37°C, 5% CO<sub>2</sub>, for 24 hours with bone marrow cultures from n=4 individual mice. Movies of 60-s duration (120 frames of 0.5 s) were recorded with a charge-coupled device camera on a Leica DMI6000 B (10× objective).

### Alveolar and peritoneal macrophage culture

Peritoneal cells were obtained by peritoneal wash with 2 ml of RPMI 1640, whereas alveolar macrophages (AMs) were obtained within the procedure of BALF. Total murine peritoneal cells as well as AMs were incubated in complete medium containing RPMI 1640 with 10% fetal bovine serum (FBS), 2 mM L-glutamine, penicillin/streptomycin (100 U/ml), and gentamicin (10 ng/ml; all from Thermo Fisher Scientific) at 37°C and 5%  $\rm CO_2$  for 4 to 5 hours, before rigorous washing with warm PBS and medium replenishment was performed. Adherent macrophages were stimulated for 10 min with calcium ionophore A23187 (5  $\mu$ M, Merck Chemicals) at 37°C and centrifuged at 4°C for harvest of supernatants for enzyme immunoassay (EIA). Cell pellets were collected, lysed, and stored as described for MDMs and BMDMs.

## **PBMC culture and stimulations**

Two to  $2.5 \times 10^5$  PBMCs per well were resuspended in RPMI 1640 medium (Thermo Fisher Scientific) supplemented with 10% fetal calf

serum (Sigma-Aldrich) and 1% penicillin/streptomycin (Thermo Fisher Scientific) and left untreated as control or stimulated with heGDH (5 µg/ml) alone or in combination with 10 µM mPGES1 inhibitor, 934, for 72 hours at 37°C in a 5% CO<sub>2</sub> atmosphere to assess  $T_{\rm reg}$  induction (CD4<sup>+</sup>CD127<sup>-</sup>CD25<sup>hi</sup>FoxP3<sup>+</sup> cells) (*18*). For SEA stimulation, 2 to 2.5  $\times$  10<sup>5</sup> PBMCs were left untreated (control) or cultured with SEA (50 µg/ml), prepared from *S. mansoni* eggs as previously detailed (*61*), alone or in combination with either heGDH (5 µg/ml) and/or 10 µM mPGES1 inhibitor, 934, for 5 days. On day 3, 50% of culture medium was exchanged with fresh medium containing respective stimuli or culture medium as control. Culture supernatants were collected, IL-4 concentrations were determined by ELISA, and cells were harvested, washed, and IL-4<sup>+</sup>CD4<sup>+</sup>  $T_{\rm H2}$  cells characterized using FACS. The gating strategy for  $T_{\rm reg}$  induction has been reported previously (*18*).

## Monocyte-naive CD4<sup>+</sup>T cell coculture and T<sub>reg</sub> induction by heGDH

Monocyte isolation from human PBMCs was performed using the Pan Monocyte Isolation Kit (Miltenyi Biotec), and autologous naive CD4<sup>+</sup> T cells were enriched with the naive CD4<sup>+</sup> T cell isolation kit II, human (Miltenyi Biotec) strictly according to the manufacturer's protocol. The purity of monocytes ( $\geq 90\%$ ) was evaluated by FACS staining with CD14 (clone HCD14) (BioLegend). Purified naive CD4<sup>+</sup> T cells (2  $\times$  10<sup>5</sup> cells) were cocultured with heGDH (5  $\mu g/ml$ ) in the absence or presence of monocytes for 72 hours, and  $T_{reg}$  induction (CD4<sup>+</sup>CD127<sup>-</sup>CD25<sup>hi</sup>FoxP3<sup>+</sup> cells) was characterized using FACS (18). For monocyte (2  $\times$  10<sup>5</sup> cells)–T cell coculture, a ratio of 1:2 monocyte/naive T cells was used.

## LDH cytotoxicity assay

Cellular cytotoxicity of stimulation with the p300 HAT inhibitor A485 in MDMs and BMDMs was quantified using the LDH cytotoxicity assay kit (Thermo Fisher Scientific) according to the manufacturer's instructions.

## Co-IP of CD64 and heGDH

IP was done with 1.5 μg of HA-heGDH and 1.5 μg of His-CD64 (Thermo Fisher Scientific) in 25 mM Hepes-NaOH (pH 7.5), 300 mM NaCl, 10% glycerol, and 0.04% Triton X-100. Twenty-five-microliter bead slurry of anti-HA magnetic beads (Thermo Fisher Scientific) or isotype control magnetic beads (MBL International) were added to the protein solution. Before IP, beads were equilibrated in the IP buffer. IP was done for 3 hours at 4°C while rotating. After IP, flow-through was collected, and beads were washed twice with 1 ml of IP buffer before proteins were eluted by adding 20 µl of 2× Laemmli and heating for 5 min at 95°C. After heating, the supernatant was collected, and 5% of β-mercaptoethanol was added. Flow-through and wash were reconcentrated with Amicon Ultra-0.5, Ultracel-3 Membrane, 3 kDa (Merck Millipore) to approximately 20 μl. A total of 5× Laemmli  $+\beta$ -mercaptoethanol was added, and the reconcentrated samples were heated for 5 min at 95°C. Samples were loaded on a 4 to 20% bis-tris gel (GenScript) and analyzed via protein immunoblot.

## **Protein immunoblot**

The protein concentration was determined by the bicinchoninic acid (BCA) method (Thermo Fisher Scientific), and lysates were diluted to equal concentrations between 12 and 20  $\mu$ g. NuPAGE LDS sample buffer and NuPAGE sample reducing agent (Thermo Fisher Scientific)

were added to total lysates and heated at 95°C for 5 min. Samples were loaded on Bolt 4 to 12% bis-tris Plus gels (Thermo Fisher Scientific) and separated by electrophoresis. Gels were transferred to a polyvinylidene difluoride membrane (Merck Chemical) and blocked in 5% nonfat dry milk in 1× tris-buffered saline containing 0.05% Tween for several hours to prevent nonspecific binding. Membranes were incubated overnight with primary antibodies against H3K27ac (Diagenode; dilution 1:1000), β-actin (Sigma-Aldrich, Merck; dilution 1:10,000), heGDH (4F8; dilution 1:1000), or His<sub>6</sub> tag (Thermo Fisher Scientific; dilution 1:250), washed, and incubated with the corresponding secondary horseradish peroxidase-conjugated antibody (dilution 1:10,000). Detection was performed using enhanced chemiluminescence (SuperSignal West Femto Maximum Sensitivity Substrate, Pierce, Thermo Fisher Scientific) and recorded with the ECL Chemocam Imager (Intas Science Imaging Instruments). When indicated, ImageJ software was used to quantify the protein concentrations by means of normalization and correction for  $\beta$ -actin in the samples.

## siRNA knockdown of p300 HAT in MDMs and BMDMs

A total of  $4\times10^5$  cells were seeded in a 12-well plate. MDMs and BMDMs were transfected with 100 and 25 nM siRNA, respectively. The transfection approach contained serum-free medium, p300 siRNA (Horizon Discovery), and 3% HiPerFect Transfection Reagent (QIAGEN). After 6 hours, MDMs were supplemented with medium containing GM-CSF, TGF- $\beta$ , and heGDH. IF staining was performed 48 hours after transfection. For BMDMs, medium was discarded and replaced after 6-hour incubation. heGDH stimulation was done on the next day. After treatment for 24 hours with heGDH, IF staining was performed.

## Flow cytometry (FACS) analysis

MLNs of Nb- or Hpb-infected mice were removed and transferred in RPMI 1640 medium on ice until further processing for FACS analysis. The lungs of Nb-infected mice were removed and digested using collagenase (1 mg/ml; Sigma-Aldrich, Merck) and deoxyribonuclease I (DNase I; 0.1 mg/ml; STEMCELL Technologies) for 30 min at 37°C. Cells of the MLN and lung were forced through a 70-μm cell strainer using cold PBS for MLN or cold FACS buffer (PBS with 5 mM EDTA and 1% of FBS) for the lung to prepare a single-cell suspension. The cell suspension (one-fourth) from MLNs was lysed in RLT buffer with 1% β-mercaptoethanol (Merck Millipore) and stored at -70°C for RNA extraction. Lung cells were further treated for 1 min with ammonium-chloride-potassium (ACK) buffer to lyse erythrocytes. Lysis was stopped by adding 10 ml of RPMI containing FBS. Lung cells were centrifuged, and pellet was resuspended in 40% Percoll (GE Healthcare). The 40% Percoll-cell suspension was layered on top of 80% Percoll and centrifuged for 15 min at RT without brake. After density separation, leukocytes were collected from the interphase and washed once again in PBS. T cell populations from the MLN or lung were stained extracellularly with CD3 (AF700, BioLegend) and CD4 (fluorescein isothiocyanate, BioLegend) after a 10-min incubation to block Fc receptors [TruStain FcX (anti-mouse CD16/32) antibody, BioLegend]. Next, cells were fixed and permeabilized for 30 min using a Fixation/Permeabilization kit (Thermo Fisher Scientific) and before intracellular staining of Foxp3 [phycoerythrin (PE)-cyanine (Cy) 5.5, eBioscience, Gata3 (EF660, eBioscience), Helios [Pacific Blue (PB), BioLegend], and Roryt (PE, eBioscience) was performed. EP2<sup>-/-</sup> BMDMs were stained against CD206 (PE-Cy7, BioLegend). Live/dead aqua (Life Technologies) was used for all

cells to exclude dead cells from the analysis. Samples were acquired on a BD LSRFortessa (BD Biosciences) and analyzed using FlowJo v10 software (FlowJo LLC).  $T_{reg}$  induction was characterized as CD3<sup>+</sup>CD4<sup>+</sup>CD127<sup>-</sup>CD25<sup>hi</sup>FoxP3<sup>+</sup> cells and  $T_{H2}$  cells as IL-4<sup>+</sup>CD4<sup>+</sup> T cells as previously described (*18*) with the following antihuman antibodies: CD3 (BV510, BioLegend), CD4 (BV421, BioLegend), CD127 (BV605, BioLegend), CD25 (PE-Dazzle 594, BioLegend), Foxp3 [allophycocyanin (APC), Invitrogen], and IL-4 (PE/Cy7, BioLegend).

## Histology and IF staining

For histology, the proximal 5 cm of the small intestine of *Nb*- or *Hpb*-infected mice was freed from mucus, extensively washed with cold PBS supplemented with penicillin and streptomycin (200 U/ml), and then rolled into "Swiss rolls." The lungs of *Nb* experiments and Swiss rolls of *Hpb*- and *Nb*-infected mice were placed in a tissue cassette and fixed in 3.7% formaldehyde before standard formalin-fixed, paraffinembedded (FFPE) processing. Swiss rolls of *Hpb*-infected mice that were scarified 4 days p.i. were placed in cryo-molds and embedded in Tissue-Tek optimum cutting temperature compound (Science Services) and then frozen on dry ice.

Sections of all tissues were cut and stained with hematoxylin and eosin. Images were recorded with the EVOS system. Linear means intercept (Lmi) was quantified as a score of *Nb*-driven lung damage in a blinded fashion, as described previously (6). Briefly, sections of lung were viewed by microscopy with an original magnification of ×200; 15 random non-overlapping fields per sample were assessed. Six horizontal lines were drawn across each image, and the total number of times the alveolar wall intercepted per line was counted. Line length was then divided by the number of intercepts to calculate Lmi.

FFPE tissues for IF and immunohistochemistry staining of the *Hpb*-infected intestine were first deparaffinized and rehydrated after heating at 65°C for 10 min twice with Roticlear and isopropanol and once with 90 and 70% ethanol. To reduce the autofluorescence background on FFPE and rehydrated cryosections, MaxBlock Autofluoresence Reducing Reagent (MaxVision Bioscience) was used. Before both stainings, antigen retrieval by repeated boiling in sodium citrate buffer + 0.05% Tween 20 was performed. Subsequently, tissue was permeabilized and blocked with 3% bovine serum albumin and 10% donkey serum at RT. Tissues for immunohistochemistry staining were further blocked with the Avidin/Biotin Blocking Kit (Thermo Fisher Scientific).

For IF staining of MDMs or BMDMs, cells were seeded on 8- or 12-well glass chamber slides (Ibidi) and stimulated for the indicated time points. After treatment, cells were fixed for 15 min with 4% paraformaldehyde (Sigma-Aldrich, Merck), followed by permeabilization with acetone (10 min at  $-20^{\circ}$ C). After the same blocking procedure, cells or tissues were incubated with primary antibodies against goat anti-actin (Santa Cruz Biotechnology), goat anti-COX-2 (Cayman Chemical), goat anti-myeloperoxidase (R&D Systems), mouse anti-CD64 (Thermo Fisher Scientific), mouse anti-mPGES1 (Cayman Chemical), rabbit anti-15 Lipoxygenase 1 (Abcam), rabbit anti-Arg1 (Abcam), rabbit anti-CD64 (Thermo Fisher Scientific), rabbit anti-p300 (Cell Signaling), rabbit anti-RELMα (PeproTech), rabbit anti-Ym1 + Ym-2 (Abcam), rabbit immunoglobulin G (IgG) isotype control (Thermo Fisher Scientific), rat anti-CD64 (BioLegend), rat anti-iNOS (Thermo Fisher Scientific), or rat IgG2a monoclonal isotype control antibody (BioCell). For staining of heGDH,

the α-heGDH mAb (clone 4F8) was used. Where indicated, blocking of  $\alpha$ -heGDH mAb with its antigen peptide was performed in a ratio of 1:1 overnight at 4°C while rotating. Fluorescence-conjugated secondary antibodies (Thermo Fisher Scientific) were used for detection of IF staining. Before images were recorded on a Leica SP5 confocal microscope (Leica Microsystems), on a Zeiss LSM 800, or a Nanozoomer slide scanner, cells were mounted and stained with Fluoroshield containing 4',6-diamidino-2-phenylindole (DAPI; GeneTex). For immunohistochemistry staining, the RELMα, biotinylated antimurine antibody (PeproTech), or the anti- $\alpha$ -SMA antibody (Abcam) was used. A biotin-conjugated secondary antibody (Thermo Fisher Scientific) was used to stain anti- $\alpha$ -SMA. Detection and development were performed by applying ABC Peroxidase Standard Staining (Thermo Fisher Scientific) and the 3,3'-diaminobenzidin (DAB) Enhanced Liquid Substrate System (Sigma-Aldrich, Merck). Before recording with the EVOS system, nuclear counterstain and mounting were done. Files were adjusted equally for brightness and contrast using ImageJ. For the quantification of Ym-1/2 (IF staining) or RELMa (IF or DAB staining), the secondary antibody staining control images were used as background. All areas with a higher intensity compared with the secondary control were considered as "true" staining. The intensity and area of staining were calculated as the percentage. The image with the most intensive (the average value of the brightness of all pixels) staining was assumed to be 1. Quantification was done using HALCON (MVTec Software GmbH).

### Masson trichrome staining

Sections were stained at University of Lausanne, Department of Immunobiology at the Histology facility. In short, FFPE tissue sections of Hpb- and Nb-infected intestines were first deparaffinized and rehydrated. Tissues were fixed at 60°C in a preheated Bouin solution for 30 min. Sections of all tissues were stained with hematoxylin and differentiated in acid alcohol. Afterward, sections were rinsed under running tap water until blue became visible. Next, Biebrich scarlet acid fuchsin staining was used for 2 min before phosphomolybdic acid/phosphotungstic acid staining for 12 min. At the end, tissues were covered in methyl blue and differentiated in 1% acetic acid before dehydration and mounting. Quantification of Masson trichrome staining in lungs from Nb-infected mice was done by segmenting the blue areas. The intensity and the area of blue staining were calculated as the percentage. The image with the most intensive blue staining was assumed to be 1. Quantification was done using HALCON (MVTec Software GmbH).

## **RNA** isolation

RNA from tissue (MLN) or cultivated macrophages was extracted using a spin-column kit (Zymo Research) and transcribed into DNA using the High-Capacity cDNA Reverse Transcription kit according to the manufacturer's instructions (Thermo Fisher Scientific) or submitted for total RNA-seq.

## Collection and RNA isolation of different H. polygyrus stages

For RNA extraction, 5000 viable L3 larvae were used. Fourth-stage larvae (L4) were collected 5 days p.i. using a Baerman apparatus. L5-stage *Hpb* worms were obtained from the intestine of mice 15 days p.i. All parasite life cycle stages underwent two washes with penicillin-streptomycin (100 U/ml) and were subsequently lysed by adding 1 ml of TRIzol. Homogenization was achieved using Lysing Matrix D tubes (MP Biomedicals) in Fast-Prep-24TM5G for 120 s at 8 m/s.

The mixture was then incubated for 5 min at RT, followed by the addition of 0.2 ml of cold chloroform. After mixing and incubation at RT for 3 min, samples were centrifuged at 12,000g for 15 min at 4°C. The clear upper phase was carefully transferred to a new Eppendorf tube, and an equal volume of 100% ethanol was added. This mixture was then processed using the RNA Clean & Concentrator-25 kit (Zymo Research), following the manufacturer's instructions. Genomic DNA was digested with DNase I during the isolation protocol. Obtained RNA was reverse-transcribed into DNA (see the "RNA isolation" section). For quantitative reverse transcription PCR, a 10-ng cDNA template with primers for heGDH\_v1 and heGDH\_v2 was used. The mean of CT values given for both primer pairs was calculated. A list of primers (4  $\mu$ M, Sigma-Aldrich, Merck) is shown in table S2.

## **Quantitative reverse transcription PCR**

FastStart Universal (Roche, Mannheim) or PowerUp (Thermo Fisher Scientific) SYBR Green master mixes were used for the 10-ng cDNA template, and qPCR was performed on the ViiA7 Real-Time PCR, QuantStudio 5 System (Applied Biosystems; Thermo Fisher Scientific) or the LightCycler 480 Real-Time PCR System (Roche). For AMs, a 6.8-ng cDNA template was used. The expression levels were normalized to *GAPDH* for MDMs, BMDMs, and AMs or to *Actb* for MLN as housekeeping gene, and relative gene expression was represented as  $2^{-\Delta CT}$  [ $\Delta CT = \Delta CT_{\text{(gene)}} - CT_{\text{(housekeeper)}}$ ]. For genes where expression could not be quantified, CT values were set to 40. A list of primers (4  $\mu$ M, Metabion or Sigma-Aldrich, Merck) is shown in table S2.

## RNA sequencing

Sequencing of RNA from MDMs treated with heGDH was performed at the Helmholtz Munich by the Genomics Core Facility. The preparation of samples, library preparation, and sequencing were done as previously described (62, 63). Library preparation was performed using the TruSeq Stranded mRNA Library Prep Kit (Illumina). Quality and quantity of RNA were assessed by a Qubit 4 Fluorometer (Invitrogen), and RNA integrity number was determined with the Agilent 2100 BioAnalyzer (RNA 6000 Nano Kit, Agilent). For library preparation, 1 μg of RNA was poly(A)-selected, fragmented, and reverse-transcribed with the Elute, Prime, Fragment Mix (Illumina). A-tailing, adaptor ligation, and library enrichment were performed as described in the TruSeq Stranded mRNA Sample Prep Guide (Illumina). RNA libraries were assessed for quality and quantity with the Agilent 2100 BioAnalyzer and the Quant-iT PicoGreen dsDNA Assay Kit (Life Technologies, Thermo Fisher Scientific). RNA libraries were sequenced as 150-bp paired-end runs on an Illumina NovaSeq 6000 platform. Reads were aligned to hg18 with the Genomic Short-read Nucleotide Alignment Program (GSNAP), and FeatureCounts was used to assign the reads to genes as previously described (62).

## RNA-seq data processing

Further analysis on the RNA-seq count matrix was carried out using R. Genes with fewer than a total count of 100 across all of the samples were filtered out. Then, genes that had at least 10 counts in all samples were kept. The variance-stabilizing transformation (vst) (64) normalization implemented in the DESeq2 (65) package was used to normalize the filtered RNA-seq counts. The DESeq2 package was used to calculate the fold change (FC), base mean, and adjusted *P* values of the DEGs for the following contrasts: LPS-treated versus PBS-treated, heGDH-treated versus LPS-treated, and heGDH-treated versus

PBS-treated. Subsequently, the pheatmap package (CRAN, 2015) was used to plot heatmaps of the top 50 genes with the largest log<sub>2</sub> FC with at least 50 base counts in the above-mentioned contrasts. In addition, the EnhancedVolcano package was used to create volcano plots of the DEGs with at least 50 base counts (https://github.com/kevinblighe/EnhancedVolcano).

## Lipid mediator quantification via LC-MS/MS of cellular (MDM and BMDM) supernatants

Eicosanoids in intestinal culture supernatants, BALF, and supernatants of cultured macrophages were quantified by LC-MS/MS using previously published protocols (66-68). Automated solid-phase extraction was performed on a Microlab STAR robot (Hamilton). Before extraction, all samples were diluted with H<sub>2</sub>O to a MeOH content of 15%, and internal standard was added. Samples were extracted using Strata-X 96-well plates (30 mg, Phenomenex). After elution with MeOH, samples were evaporated to dryness under N<sub>2</sub> stream and redissolved in MeOH/H<sub>2</sub>O (1:1). Chromatographic separation of eicosanoids was achieved with a 1260 Series high-performance liquid chromatography (HPLC) (Agilent) using a Kinetex C18 reversed-phase column (2.6 µm, 100 mm by 2.1 mm, Phenomenex) with a SecurityGuard Ultra Cartridge C18 (Phenomenex) precolumn. The QTRAP 5500 mass spectrometer (Sciex), equipped with a Turbo V ion source, was operated in negative ionization mode. Samples were injected via an HTC PAL autosampler (CTC Analytics), set to 7.5°C. Identification of metabolites was achieved via retention time and scheduled multiple reaction monitoring as previously specified. Acquisition of LC-MS/MS data was performed using Analyst Software 1.6.3 followed by quantification with MultiQuant Software 3.0.2 (both from Sciex).

## LC-MS/MS quantification of prostanoids in cultured macrophage supernatants

This method was used for data in Fig. 4 (B and C). LC-MS/MS analysis of prostanoids in supernatant samples was performed as described previously (66) with slight modifications. Briefly, a volume of the 200-µl cultured macrophage supernatant was extracted using liquid-liquid extraction with 600 µl of ethyl acetate after adding 20 µl of internal standard solution (PGE<sub>2</sub>-d4, PGD<sub>2</sub>-d4, TXB<sub>2</sub>-d4, PGF<sub>2α</sub>-d4, and 6-keto PGF<sub>1α</sub>d4, all purchased from Cayman Chemical) and 100 μl of 0.15 M EDTA solution. In the case of a smaller sample volume, supernatant samples were filled up with PBS. The extraction step was repeated, and organic layers of both extraction steps were combined, evaporated at 45°C under a gentle stream of nitrogen, and reconstituted with 50  $\mu$ l of acetonitrile/water/formic acid (20:80:0.0025, v/v). Ten microliters of the resuspended sample was injected into the LC-MS/MS system. The LC-MS/MS system consisted of an Agilent 1290 LC system (Agilent) coupled to a 6500+ QTRAP tandem mass spectrometer (Sciex) equipped with a Turbo V source operating in negative electrospray ionization mode. Chromatographic separation was achieved using a Synergi Hydro-RP column (2.0 mm by 150 mm, 4-µm particle size, Phenomenex), equipped with a precolumn of the same material. Mobile phases A and B were 0.0025% formic acid and acetonitrile with 0.0025% formic acid. Chromatographic separation was achieved under gradient conditions. For analysis, Analyst Software 1.7.1 and Multiquant Software 3.0.3 (both from Sciex, Darmstadt, Germany) were used, using the internal standard method (isotope dilution mass spectrometry). The necessary standard curves were created using PBS as a surrogate matrix.

## LC-MS/MS quantification of lipid mediators in intestinal culture supernatants

The determination of prostanoids and hydroxyeicosatetraenoic acids (HETEs) in intestinal culture supernatants was performed in a similar manner as described for the determination of prostanoids in cultured macrophage supernatants. In addition to the mentioned internal standards for the determination of prostanoids, additional internal standards were used for the HETEs (5S-HETE-d8, 12S-HETE-d8, and 15S-HETE-d8, all purchased from Cayman Chemical). The sample preparation followed the same procedure as described above. In the case of sample dilution, PBS was used. However, after evaporation, the sample was reconstituted in 50 µl of MeOH/water (70:30) containing 0.0001% butylhydroxytoluol (BHT). The equipment and software used for data acquisition and analysis also correspond to the description above. However, an Acquity UPLC BEH C17 100 mm-by-2.1 mm, 1.7-µm chromatography column with a corresponding guard column was used. Gradient elution was also used for this analysis.

## LC-MS/MS quantification of lipid mediators in BAL supernatants

Briefly, BALF supernatants, stored in an equal volume of MeOH, were extracted using solid-phase extraction (Evolute Express ABN, Biotage, Uppsala, Sweden), and lipid mediators were quantified by LC-MS/MS as published previously (63, 67, 68).

## **Enzyme immunoassays**

The concentration of cysLTs and PGE<sub>2</sub> in culture supernatants was determined using commercially available EIA kits (Cayman Chemical), according to the manufacturer's instructions.

## **Enzyme-linked immunosorbent assay**

Cytokines were quantified using commercially available ELISA kits according to the manufacturer's instructions. MDM supernatants were analyzed for IL-10 or IL-12 $\beta$  secretion using the human IL-10 ELISA Set (BD Biosciences) or the human IL-12/IL-23 p40 DuoSet ELISA (R&D Systems). BMDM supernatants were analyzed for IL-10 using the mouse IL-10 DuoSet ELISA (R&D Systems). PBMC supernatants were analyzed for IL-4 using the IL-4 human ELISA kit (Thermo Fisher Scientific).

## Chromatin immunoprecipitation

For ChIP with formaldehyde cross-linking, macrophages (3 to 5 × 10<sup>6</sup> cells per condition) were incubated for 30 min at 37°C and 5% CO<sub>2</sub> with Accutase (Sigma-Aldrich, Merck) to detach the cells. ChIP protocol steps were performed similar to previously described (69). Fragmentation of the chromatin was carried out using a focused ultrasonicator (Covaris) for 15 min at 6°C with a peak power of 140 W, 5% duty factor, and 200 cycles per burst. Instead of agarose beads, ChIP-grade protein A/G magnetic beads (Thermo Fisher Scientific) were added to the chromatin and antibody mixture, and incubation was done for 2 hours at 4°C while rotating. DNA purification was performed with the MinElute PCR Purification Kit (QIAGEN). Eluted DNA was either subjected to ChIP-seq or used for ChIP-qPCR experiments. Input chromatin DNA was prepared from one-fourth of the chromatin amount used for ChIP. Antibodies used for ChIP were anti-H3K27ac and isotype control antibody (both 4 μg from Abcam).

## Chromatin immunoprecipitation sequencing

ChIP-seq was performed at the European Molecular Biology Laboratory (EMBL, Heidelberg) by the Genomics Core Facility. Samples were prepared for sequencing using the DNA Ultra II kit (New England Biolabs Inc.) as per the manufacturer's instructions. Briefly, samples were split into two groups on the basis of the amount of the material. Samples for which the material could be detected with the Qubit DNA High Sensitivity Assay (Thermo Fisher Scientific) were standardized to 4-ng input. Sequencing adapters were diluted 1:25 before ligation, and 16 cycles of PCR were used. For samples for which no material was detected (isotype control IgG IP samples), 8 μl was taken into the protocol, with adapter dilution of 1:25 and 20 PCR cycles. Size selection was performed according to New England Biolabs (NEB) recommendations for 300 to 400 base pairs, using solid-phase reversible immobilization (SPRI) beads (Beckman Coulter). Finished libraries were pooled equimolarly according to concentration measured by Qubit DNA High Sensitivity and size as measured by the Bioanalyzer DNA High Sensitivity assay (Agilent). Libraries were sequenced using the NextSeq 500 High flowcell (Illumina) with chemistry for 75 cycles. Sequences were base-called, and reads were demultiplexed using bcl2fastq with standard settings.

## ChIP-seq data processing

The ChIP-seq data were preprocessed using the publicly available nf-core/chip-seq pipeline (v2.0.0) with the read length 75 parameter. The reads were aligned to the National Center for Biotechnology Information (NCBI) GRCh38 reference genome (iGenomes) [Illumina (2016) *Homo sapiens* reference genome, NCBI GRCh38 version]. Peaks were called with model-based analysis of ChIP-seq 2 (MACS2) using the broadPeak mode. Data analysis was performed with R (version 4.0.3) (70). The read counts were normalized by library size and transformed to a log2-like scale using the vst function from the DeSeq2 (65) package. All plots were generated with ggplot2 (v3.4.1) (71) unless otherwise stated.

## Differential ChIP-seq analysis

Differential peaks were identified with DiffBind (v3.0.15) (72). Using DiffBind, blacklisted peaks were removed, consensus peaks of 1-kbp size were computed, and reads were normalized by library size using background windows of 10-kbp size. Significantly differential peaks were identified by false discovery rate (FDR;  $\leq$ 0.05) and absolute log<sub>2</sub> FC (>1). The peaks were annotated by finding overlaps with enhancers listed by GeneHancer (v5.13) (73). For each associated gene, the peak with the highest log<sub>2</sub> FC was selected and denoted as the most influential peak for one-to-one comparisons with RNA-seq data and visualization purposes.

## Visualization of the eicosanoid pathway

The eicosanoid pathway was visualized with Cytoscape (v3.9.1) (74). To that end, the WikiPathway WP167 was used, and nodes were highlighted with the log<sub>2</sub> FCs obtained from the differential gene expression data and the differential peak analyses.

### ChIP-seq signal visualization

Genome visualizations of the ChIP-seq signal of differential peaks were generated with trackplot and bwtool (v1.0) (75). To that end, the mean ChIP-seq signal was computed for bigwig files of heGDH and control samples, respectively, using wiggletools mean (v1.2.10) (76).

### ChIP-qPCR

ChIP-qPCR was performed with PowerUp (Thermo Fisher Scientific) SYBR Green master mix following the manufacturer's instructions. For all primer pairs, input chromatin DNA was used to generate standard curves and verify amplification efficiency between 90 and 100%. qPCR was performed on a ViiA7 Real-Time PCR System (Applied Biosystems, Thermo Fisher Scientific). Changes in enrichment at specific regions were normalized to three different positive control regions (glyceraldehyde phosphate dehydrogenase, NSA2 ribosome biogenesis homolog, and TATA box-binding protein) that did not show changes in histone modifications during stimulation with heGDH.

## Cloning, expression, and purification of heGDH, heGDH $^{\rm K126A,D204N}$ , HA-heGDH, heGDH $^{\rm C136S}$ , and heGDH $^{\rm \Delta N}$ Preparation of the expression constructs

The heGDH gene was amplified by PCR using Pfu polymerase and a pET-21a/heGDH construct (GeneArt, Thermo Fisher Scientific) as the template. The obtained PCR product was cloned into a linearized pET TrxA-1a vector, an expression vector containing N-terminal His<sub>6</sub> and thioredoxin tags followed by a tobacco etch virus (TEV) protease cleavage site using the seamless ligation cloning extract (SLiCe) method (77). For the insertion of an N-terminal HA tag to heGDH, the gene was amplified using a forward primer containing the HA tag sequence: HA-heGDH forward primer (HA tag unlined) and the heGDH reverse primer. The cloning was performed as described above.

The catalytically inactive double mutant (K126A and D204N) of heGDH and the cysteine mutant (C136S) were produced by site-directed mutagenesis using a QuikChange mutagenesis kit (Agilent). The truncated protein ( $\Delta$ N) was produced by PCR amplification using a forward primer starting at heGDH residue 34 (deleting residues 1 to 33) and the heGDH reverse primer. The PCR product was cloned into a linearized pET TrxA-1a vector. All reactions used the N-terminal His<sub>6</sub> tag heGDH construct as the template. All expression constructs were verified by sequencing.

### Protein expression and purification

The heGDH expression constructs or empty vector (mock) was transformed into E. coli strain BL21 (DE3) CC4 [overexpressing the (co-)chaperones GroEL, GroES, DnaK, DnaJ, GrpE, and ClpB] (78) and cultured overnight at 20°C in 2-liter flasks containing 500 ml of ZYM 5052 autoinduction medium (79) and kanamycin (100  $\mu$ g/ml), spectinomycin (50 μg/ml), and chloramphenicol (10 μg/ml). Cells from 2 liters of culture were harvested by centrifugation after reaching saturation, resuspended in 120 ml of lysis buffer [50 mM tris-HCl, 300 mM NaCl, 20 mM imidazole, 10 mM MgCl<sub>2</sub>, DNase I (10 μg/ml), 1 mM AEBSF.HCl, 0.2% (v/v) NP-40, lysozyme (1 mg/ ml), and 0.01% (v/v) 1-thioglycerol (pH 8.0)], and lysed by sonication. The lysate was clarified by centrifugation (40,000g) and filtration (0.2 µm). The supernatant was applied to a 5-ml HiTrap Chelating HP column (Cytiva), equilibrated in buffer A [50 mM tris-HCl, 300 mM NaCl, 20 mM imidazole, and 0.01% (v/v) 1-thioglycerol (pH 8.0)] using an Äkta Purifier (Cytiva). The column was washed with buffer A containing 50 mM imidazole until a stable baseline was reached (monitored at 280 nm). Bound proteins were eluted with a linear gradient from 50 to 300 mM imidazole in buffer A. Fractions containing heGDH were pooled and dialyzed overnight at 4°C against 1 liter of buffer B [50 mM tris-HCl, 300 mM NaCl, and 0.01% (v/v) 1-thioglycerol (pH 8.0)]. Next, 5 mM ATP (from a 100 mM stock

solution at pH 7) and 1 mM MgCl<sub>2</sub> were added, and the solution was incubated overnight at 4°C to detach bound chaperones. The solution was applied to a 5-ml HiTrap Chelating HP column, and the protein was purified as described above. Fractions containing heGDH were pooled and dialyzed overnight at 4°C against 1 liter of buffer B in the presence of His-tagged TEV protease in a 1:25 molar ratio (TEV:protein). The cleaved off heGDH was further purified by affinity chromatography as described above, and the flow-through and the protein containing wash fractions were pooled and concentrated to less than 5 ml. This was subsequently subjected to size exclusion chromatography using a HiLoad 16/600 Superdex 200 column (Cytiva), equilibrated in buffer B. The fractions containing heGDH was pooled and dialyzed overnight against 1 liter of PBS (pH 7.4) at 4°C. Last, the solution was concentrated to approximately 2 mg/ml and stored at 4°C. Given that the heGDH $^{\Delta N}$  was highly soluble compared with the other constructs, the protein solution was concentrated to 6 mg/ml. The catalytically inactive double mutant of heGDH was purified using the same protocol without the ATP-MgCl2 incubation and the second affinity chromatography step. Concentrations of the different protein constructs were determined by measuring the absorbance at 280 nm using the specific absorbances for full length heGDH of 1.060, heGDH $^{\Delta N}$  of 1.126, heGDH $^{K126A,D204N}$  of 1.061, and heGDH<sup>C136S</sup> of 1.060 ml/mg\*cm, respectively.

## Fluorochrome labeling of heGDH

heGDH was labeled with the Atto 488 Protein Labeling Kit (Sigma-Aldrich, Merck). heGDH (2 mg/ml) was mixed with the reactive dye (10 mg/ml). The reaction mixture was incubated for 1 hour at RT while shaking. Subsequently, the fluorochrome-conjugated protein was purified with a PD-10 desalting column.

### Crystallization and structural determination

Crystallization experiments were done on heGDH and heGDH $^{\Delta N}$ by sitting-drop vapor-diffusion methods at 18°C and were performed at the X-ray Crystallography Platform at Helmholtz Munich. The structure of heGDH, heGDH $^{\text{C136S}}$ , and heGDH $^{\Delta N}$  was also determined by cryo-EM SPA on a FEI Titan Krios transmission electron microscope. heGDH was concentrated to 10 mg/ml, and crystals were obtained by mixing the protein with an equal volume of precipitant containing 12% (v/v) 2-propanol, 50 mM MES (pH 6.0), 200 mM potassium chloride, and 6 mM cobalt (III) hexamine chloride. Before flash cooling, crystals were cryo-protected by soaking in mother liquor supplemented with 25% ethylene glycol. X-ray diffraction data were acquired at the Swiss Light Source (SLS, Villigen, Switzerland) at beam line PXII. All diffraction data were collected at cryogenic temperatures (100 K) at wavelengths of 1.000 Å. For the truncated version,  $\Delta N$ , the protein was concentrated to 9.5 mg/ml, and crystals were obtained by mixing the protein with an equal volume of precipitate containing 0.1 M acetic acid (pH 5.5) and 20% (v/v) 2-methyl-2,4-pentandiol (MPD). X-ray diffraction data were acquired at the European Synchrotron Radiation Facility (Grenoble, France), at the beam line ID23-2 (80). All diffraction data were collected at cryogenic temperature (100 K) at a wavelength of 0.873 Å. For both cases, the data were indexed with the X-ray Detector Software (XDS) package (81) before scaling with Aimless as part of the CCP4 package (82, 83). The structure of heGDH was determined at a resolution of 1.8 Å by molecular replacement with the human GDH [Protein Data Bank (PDB) code 111f (84)]; in the case of the truncated version, the molecular replacement model used was the solved heGDH (this publication). In both cases, the program Phaser (85) was used to find a solution, as implemented in the PHENIX software package (86). Two molecules of heGDH were found in the asymmetric unit, and the structure was completed by iterative cycles of model building in Coot (87) and refinement in PHENIX. Building the solution observed hexamer was possible by writing two related symmetry molecules (see table S3 for refinement statistics).

## **Cryo-electron microscopy**

For cryo-EM sample preparation, 4.5  $\mu$ l of the protein sample was applied to glow-discharged Quantifoil 2/1 grids, blotted for 4 s with force 4 in a Vitrobot Mark III (Thermo Fisher Scientific) at 100% humidity and 4°C, and plunge frozen in liquid ethane, cooled by liquid nitrogen. heGDH wild-type data were acquired with an FEI Titan Krios transmission electron microscope at the Department of CryoEM Technology, Max Planck Institute (MPI) Martinsried using SerialEM software (88). Movie frames were recorded using a K3 direct electron detector (Gatan) with a total electron dose of ~60 electrons per Ų distributed over 30 frames at a pixel size of 0.84 Å. Micrographs were recorded in a defocus range from -0.5 to -3.0  $\mu$ m.

For the N-terminal tail truncation ( $\Delta N$ ) and C136S mutant, data were acquired with EPU in eer-format on an FEI Titan Krios G4 at the Helmholtz Munich Cryo-EM Platform equipped with a Falcon IVi detector (Thermo Fisher Scientific) with a total electron dose of ~55 electrons per Å<sup>2</sup> and pixel sizes of 0.76 and 0.58 Å, respectively. Micrographs were recorded in a defocus range of -0.25 to -2.0  $\mu m$ .

## Cryo-EM—Image processing, classification, and refinement

For heGDH, wild-type micrographs were processed on the fly using the Focus software package (89) if they passed the selection criteria [iciness, <1.05; drift, 0.4 Å < × < 70 Å; defocus, 0.5  $\mu$ m < x < 5.5  $\mu$ m; estimated contrast transfer function (CTF) resolution, <6 Å]. Micrograph frames were aligned using MotionCor2 (90), and the CTF for aligned frames was determined using real-time CTF determination and correction (GCTF) (91). From 2565 acquired micrographs, 2,177,178 particles were picked using blob picker, two-dimensional (2D)–classified, and used for ab initio reconstruction. Three ab initio models with C3 symmetry were generated and passed through one round of heterogeneous classification. The best-performing class, containing 1,460,426 particles, was refined and yielded models with estimated resolutions of 2.3 and 2.8 Å for D3 and C1 symmetries, respectively [gold standard Fourier shell correlation (FSC) analysis of two independent half-sets at the 0.143 cutoff].

For the N-terminal tail truncation ( $\Delta N$ ) and C136S mutant, all data were processed using CryoSPARC. Micrographs were processed on the fly (motion correction and CTF estimation). Particles (2,587,398 and 350,678 for  $\Delta N$  and C136S mutant, respectively) were picked using blob picker, 2D-classified, and used for ab initio reconstruction. Final refinements of the C136S data yielded models with estimated resolutions of 2.5 and 3.0 Å for D3 and C1 symmetries, respectively (gold standard FSC analysis of two independent half-sets at the 0.143 cutoff) and 2.6 and 2.7 Å for D3 and C1 symmetries for  $\Delta N$ . Local resolution and 3D FSC plots (fig. S5) were calculated using RELION and the "Remote 3DFSC Processing Server" web interface (92), respectively.

## **GDH** activity assay

GDH activity of purified recombinant heGDH or heGDH  $^{\rm K126A,\,D204N}$  was determined both in the direction of glutamate formation and utilization. Assays were carried out at 37°C in 250  $\mu l$  of assay

mixture containing 100 mM phosphate buffer and 5 µg of protein. The enzyme activity of heGDH was determined in the direction of glutamate utilization by the rate of production of NADH/NADPH or by the rate of utilization of NADH/NADPH in the direction of glutamate formation, measured spectrophotometrically at 340 nm. The optimum pH was determined in both directions with substrate concentrations of 0.5 mM α-KG (Sigma-Aldrich, Merck) and 40 mM ammonia (Honeywell) or 5 mM glutamate (Sigma-Aldrich, Merck) with the pH range of 5.5 to 9.5. The optimum concentration of cofactors was determined using NAD(P)<sup>+</sup> concentrations (Sigma-Aldrich, Merck) from 0 to 3 mM with 4 mM glutamate or 0 to 0.8 mM NAD(P)H with 0.5 mM α-KG and 10 mM ammonia. The Michaelis-Menten constant, K<sub>m</sub>, for glutamate was determined in reaction mixtures containing 0 to 15 mM glutamate and 3 mM NAD<sup>+</sup>, and the  $K_{\rm m}$  for  $\alpha$ -KG with 0 to 1 mM  $\alpha$ -KG, 10 mM ammonia, and 0.4 mM NADH. The  $K_{\rm m}$  for ammonia was determined with 0 to 100 mM ammonia, 0.5 mM  $\alpha$ -KG, and 0.4 mM NADH. The inhibitory/ stimulatory effects of 1 mM GTP (Sigma-Aldrich, Merck), bithionol (20 μM, Focus Biomolecules), and α-heGDH mAb (1:100) on GDH activity were determined in the direction of both glutamate utilization and formation reaction. For these testing assays, the following concentrations were used: 3 mM NAD<sup>+</sup>, 0.4 mM NADH, 4 mM glutamate, 0.5 mM α-KG, and 10 mM ammonia.

## Stimulation of MDMs with HA-heGDH for proteomics

A total of  $2.5 \times 10^6$  cells were seeded in a six-well plate. MDMs were stimulated with HA-heGDH (5 µg/ml) for 30 min or 24 hours. After stimulation for the indicated time points, cells were centrifuged for 2 min at 1000g and 4°C. The supernatant was removed, and cells were washed twice with cold PBS. MDMs were lysed in lysis buffer containing 50 mM tris-HCl (pH 7.4), 150 mM NaCl, 5% glycerol, 1% NP-40, and 1 mM MgCl<sub>2</sub> with complete inhibitor cocktail (Roche Applied Science) for 20 min on ice. Lysed cells were transferred to a LoBind Tube, and cell debris were removed by centrifugation at maximum speed for 20 min and 4°C. Before IP, beads were equilibrated in wash buffer containing 50 mM tris-HCl (pH 7.4), 150 mM NaCl, 5% glycerol, 0.05% NP-40, and protease inhibitor. For the first experiment and to investigate intracellular interaction partners, an additional 5 µg of HA-heGDH was added to the lysate before IP. For the second experiment, no additional HA-heGDH was added. For both experiments, lysates were split in two for IP with anti-HA magnetic beads (Thermo Fisher Scientific) or IP with isotype control magnetic beads (MBL International). Thirty microliters of bead slurry was added to each IP approach, and IP was done for 3 hours at 4°C while rotating. After IP, beads were washed twice with wash buffer and twice with basic buffer (wash buffer without 0.05% NP-40) to get rid of detergent. Proteins were eluted by adding 1% SDS and heating for 5 min at 95°C. Proteins were analyzed via mass spectrometry.

### **Proteomics**

## Sample preparation for proteomics

Proteins were subjected to tryptic digest applying a modified filter-aided sample preparation procedure (93, 94). After protein reduction and alkylation using dithiothreitol and iodoacetamide, samples were denatured in urea buffer [8 M urea in 0.1 M tris/HCl (pH 8.5)], centrifuged on a 30-kDa cutoff filter device (Sartorius), and washed three times with UA buffer and twice with 50 mM ammoniumbicar-bonate. Proteins were proteolyzed for 2 hours at RT using 0.5  $\mu$ g of

lysyl endopeptidase (Lys-C, Wako) and subsequently for 16 hours at 37°C using 1  $\mu$ g of trypsin (Promega). Peptides were collected by centrifugation and acidified with 0.5% trifluoroacetic acid.

## Mass spectrometric measurements

LC-MS/MS analysis was performed in data-dependent acquisition mode. MS data were acquired on a Q-Exactive HF-X mass spectrometer (Thermo Fisher Scientific, Waltham, Massachusetts, USA) each online coupled to a nano-RSLC (rapid separation liquid chromatography) (Ultimate 3000 RSLC; Dionex). Tryptic peptides were automatically loaded on a C18 trap column (300 µm in inner diameter × 5 mm, Acclaim PepMap100 C18, 5 μm, 100 Å; LC Packings) at a flow rate of 30 µl/min. For chromatography, a C18 reversedphase analytical column (nanoEase MZ HSS T3 Column, 100 Å, 1.8 μm, 75 μm by 250 mm; Waters) was used at a flow rate of 250 nl/ min and following a 95-min nonlinear acetonitrile gradient from 3 to 40% in 0.1% formic acid. The high-resolution (60,000 full width at half maximum) MS spectrum was acquired with a mass range from 300 to 1500 mass/charge ratio with an automatic gain control target set to  $3 \times 10^6$  and a maximum of 30-ms injection time. From the MS prescan, the 15 most abundant peptide ions were selected for fragmentation (MS-MS) if at least doubly charged, with a dynamic exclusion of 30 s. MS-MS spectra were recorded at 15,000 resolutions with an automatic gain control target set to  $5 \times 10^2$  and a maximum of 50-ms injection time. The normalized collision energy was 28, and the spectra were recorded in profile mode.

## Proteomic data processing—Protein identification

Proteome Discoverer 2.5 software (version 2.5.0.400, Thermo Fisher Scientific; Waltham, Massachusetts, USA) was used for peptide and protein identification via a database search (Sequest HT search engine) against SwissProt human database (release 2020\_02, 20432 sequences). Search settings were 10-parts per million precursor tolerance and 0.02-Da fragment tolerance, one missed cleavage allowed. Carbamidomethylation of Cys was set as a static modification. Dynamic modifications included deamidation of Asn, Gln, and Arg; oxidation of Pro and Met; and a combination of Met loss with acetylation on protein N terminus. Percolator was used for validating peptide spectrum matches and peptides, accepting only the topscoring hit for each spectrum, and satisfying the cutoff values for FDR < 1% and posterior error probability < 0.01. The quantification of proteins was based on abundance values for unique peptides. Abundance values were normalized on the total peptide amount, and protein abundances were calculated summing up the abundance values for admissible peptides. The final protein ratio was calculated using median abundance values. The statistical significance of the ratio change was ascertained using the background-based t test approach (95). The statistic is based on the presumption that we look for expression changes for proteins that are few in comparison with the number of total proteins being quantified. The quantification variability of the nonchanging "background" proteins can be used to infer which proteins change their expression in a statistically significant manner. Immunoprecipitated proteins with increased abundance after IP with HA magnetic beads compared with IP with isotype control beads were filtered with the following criteria: Proteins were considered to be increased with an abundance above twofold, proteins identified with a single peptide were excluded, and only significant proteins were considered (P value < 0.05, P values were adjusted for multiple testing by Benjamini-Hochberg correction). In

addition, at least two MS/MS identifications had to be identified to include the protein ratio.

## Metabolic flux analysis (Seahorse assay)

A total of  $5 \times 10^4$  cells were plated per well on a Seahorse Miniplate (Agilent Technologies, Santa Clara, California). Stimulation of MDMs with heGDH (5 μg/ml) was done for 24 hours, whereas BMDMs were treated for 6 hours before the mitochondrial stress test (Agilent). MDMs and BMDMs were cultured on Seahorse Miniplates (Agilent). On the day of assay, medium was exchanged to the Seahorse XF RPMI medium (pH 7.4) (Agilent) containing 10 mM glucose (Sigma-Aldrich, Merck), 1 mM pyruvate, and 2 mM L-glutamine (both from Thermo Fisher Scientific). The Mito Stress Test (Agilent) was performed according to the manufacturer's instructions with subsequent injections of 1 µM oligomycin (Agilent), 1 µM carbonyl cyanide ptrifluoromethoxyphenylhydrazone (FCCP) for MDMs and 5 μM FCCP for BMDMs (Agilent), and 0.5 µM rotenone and antimycin A (both from Sigma-Aldrich, Merck). After the assay was performed, cells were lysed in 40 µl of RIPA buffer (Thermo Fisher Scientific), and protein concentration was determined for normalization (Pierce BCA protein assay kit, Thermo Fisher Scientific).

## Targeted quantification of amino acid and TCA cycle intermediates

A total of  $5 \times 10^5$  MDMs were plated and stimulated with heGDH (5 μg/ml) for targeted metabolomics. Metabolite quantification by LC-MS/MS was performed at the Metabolomics Core Facility of the Max Planck Institute for Immunobiology and Epigenetics in Freiburg. Metabolites were extracted from cell pellets using ice-cold 80:20 MeOH:water solution followed by LC separation [Agilent 1290 Infinity II UHPLC inline using a Phenomenex Luna propylamine column (50 mm by 2 mm, 3-µm particles)] with a solvent gradient of 100% buffer B (5 mM ammonium carbonate in 90% acetonitrile) to 90% buffer A (10 mM NH<sub>4</sub> in water) and a flow rate from 1000 to 750 µl/min. Autosampler temperature was 5°C, and injection volume was 2 µl. Mass spectrometry was performed using an Agilent 6495 QQQ-MS operating in multiple reaction monitoring (MRM) mode, and MRM setting was optimized separately for all compounds using pure standards. Data were processed using an in-house R script.

## **Activity assay of human recombinant LTC4S**

The recombinant LTC4S activity assay was done as previously described (96). To determine the effect of heGDH or L-2-HG on the activity of LTC4S, preincubations with 1 or 3 µg of heGDH or 1 mM L-2-HG were performed. Incubations were carried out with 100 ng of recombinant human LTC4S and 26 μM leukotriene A4 (LTA<sub>4</sub>) in 100 μl of 25 mM tris-HCl (pH 7.8) containing 0.03% of *n*-dodecylβ-D-maltoside and 5 mM glutathione for 15 s at RT. To determine the effect of heGDH or L-2-HG on the activity of LTC4S, preincubations with 1 or 3 µg of heGDH or 1 mM L-2-HG were performed for 3 or 30 min on ice, followed by the incubation with LTA<sub>4</sub>. Preincubations with 1 µM TK05, a potent inhibitor of LTC4S, for 3 min on ice were performed in parallel. Reactions were stopped by addition of 2 volumes of MeOH containing 300 pmol of PGB<sub>2</sub> as an internal standard followed by 1 volume of water. Produced LTC<sub>4</sub> was quantified using the reverse-phase HPLC approach. Samples were analyzed on a 3.9 mm-by-150 mm column (C18; Nova-Pak Waters) by eluting products at a flow rate of 1 ml/min with acetonitrile/MeOH/

water/acetic acid at a ratio of 30:30:40:0.1 (vol/vol) at pH 5.6. Absorbance was monitored at 280 nm. On the basis of the produced LTC<sub>4</sub>, the specific activity of LTC4S was determined as picomoles of LTC<sub>4</sub> produced by 1 ng of LTC4S in 1 min.

## LTC4S activity in differentiated MM6 homogenates

For cell-based assays, MM6 cells (0.3 to  $0.4 \times 10^6$  cells/ml) were differentiated with 50 nM 1α,25-dihydroxyvitamin D3 and TGF-β1 (5 ng/ml) in the medium for MM6 cells [RPMI 1640 with 10% FBS, penicillin/streptomycin (100 U/ml), 1% OPI-media supplement, 1× minimum essential medium nonessential amino acid solution, and 2 mM L-glutamine] for 96 hours at 37°C and 5% CO<sub>2</sub>. To check the effect of heGDH on the LTC4S activity in cell homogenates,  $3 \times 10^6$  differentiated MM6 cells were resuspended in 0.5 ml of 1× PBS and incubated with 5 μg of heGDH for 24 hours at 37°C and 5% CO<sub>2</sub>. Controls with PBS were prepared in parallel. Cell suspensions were collected and sonicated three times for 5 s on ice in the presence of 1 mM EDTA using the VCX 130 Vibra-Cell Ultrasonic Liquid Processor. Next, cell sonicates were preincubated for 30 s at 37°C followed by the incubation with 5  $\mu$ M LTA<sub>4</sub> for 10 min at 37°C. Incubations were quenched with 0.5 ml of MeOH containing 300 pmol of PGB<sub>2</sub> as the internal standard and acidified to pH 3 to 4 with 10 µl of 3 N HCl. Cell debris were removed by centrifugation at 10,000g for 10 min at 4°C. Supernatants were carried to new vials and diluted with 2 volumes of pure water before the solid-phase extraction with Oasis HLB 3 cc (Waters) cartridges. Samples were eluted with MeOH and taken to dryness under controlled nitrogen flow with TurboVap LV system (Biotage). Lipids were redissolved in 400 µl of MeOH:water (1:1) mixture before the reverse-phase HPLC. The formation of LTC4 was analyzed as described for the activity assay of human LTC4S.

## Statistical analyses

Data were analyzed by GraphPad Prism software. For LC-MS/MS (lipid mediator) and ELISA (cytokines) data, missing values below the lower limit of detection were interpolated using one-fourth of the minimum value for each metabolite. Statistical analysis of two group comparisons was performed using Mann-Whitney (unpaired), Wilcoxon test (paired), or t test depending on normal distribution. For comparison of more groups, repeated-measures (RM) one-way analysis of variance (ANOVA), Friedman test (paired), or Kruskal-Wallis test (unpaired) with Dunn correction was used with correction for multiple comparisons. P < 0.05 was considered statistically significant. Details of statistical tests and sample size are provided in the figure legends. Heatmaps were generated by R (RNA-seq data) or with the Broad Institute's Morpheus software.

## **Supplementary Materials**

The PDF file includes:

Figs. S1 to S11 Legend for movie S1 Legend for table S1 Legends for data files S1 and S2 Tables S2 to S4

Other Supplementary Material for this manuscript includes the following:

Movie S1
Table S1
Supplementary file for Immunoblots
Data files S1 and S2
MDAR Reproducibility Checklist

### **REFERENCES AND NOTES**

- P. M. Jourdan, P. H. L. Lamberton, A. Fenwick, D. G. Addiss, Soil-transmitted helminth infections. *Lancet* 391, 252–265 (2018).
- A. F. R. Neto, Y. L. Di Christine Oliveira, L. M. de Oliveira, R. La Corte, S. Jain,
   D. P. de Lyra Junior, R. T. Fujiwara, S. S. Dolabella, Why are we still a worm world in the 2020s? An overview of risk factors and endemicity for soil-transmitted helminthiasis. *Acta Parasitol.* 68, 481–495 (2023).
- R. M. Maizels, H. H. Smits, H. J. McSorley, Modulation of host immunity by helminths: The expanding repertoire of parasite effector molecules. *Immunity* 49, 801–818 (2018).
- R. M. Anthony, J. F. Urban Jr., F. Alem, H. A. Hamed, C. T. Rozo, J.-L. Boucher, N. Van Rooijen, W. C. Gause, Memory T(H)2 cells induce alternatively activated macrophages to mediate protection against nematode parasites. *Nat. Med.* 12, 955–960 (2006).
- J. Esser-von Bieren, I. Mosconi, R. Guiet, A. Piersgilli, B. Volpe, F. Chen, W. C. Gause, A. Seitz, J. S. Verbeek, N. L. Harris, Antibodies trap tissue migrating helminth larvae and prevent tissue damage by driving IL-4Rα-independent alternative differentiation of macrophages. PLOS Pathoq. 9, e1003771 (2013).
- T. E. Sutherland, N. Logan, D. Rückerl, A. A. Humbles, S. M. Allan, V. Papayannopoulos, B. Stockinger, R. M. Maizels, J. E. Allen, Chitinase-like proteins promote IL-17-mediated neutrophilia in a tradeoff between nematode killing and host damage. *Nat. Immunol.* 15, 1116–1125 (2014)
- F. Chen, W. Wu, A. Millman, J. F. Craft, E. Chen, N. Patel, J. L. Boucher, J. F. Urban, C. C. Kim, W. C. Gause, Neutrophils prime a long-lived effector macrophage phenotype that mediates accelerated helminth expulsion. *Nat. Immunol.* 15, 938–946 (2014).
- F. Chen, D. W. El-Naccache, J. J. Ponessa, A. Lemenze, V. Espinosa, W. Wu, K. Lothstein, L. Jin, O. Antao, J. S. Weinstein, P. Damani-Yokota, K. Khanna, P. J. Murray, A. Rivera, M. C. Siracusa, W. C. Gause, Helminth resistance is mediated by differential activation of recruited monocyte-derived alveolar macrophages and arginine depletion. *Cell Rep.* 38, 110215 (2022).
- J. D. Turner, N. Pionnier, J. Furlong-Silva, H. Sjoberg, S. Cross, A. Halliday, A. F. Guimaraes, D. A. N. Cook, A. Steven, N. Van Rooijen, J. E. Allen, S. J. Jenkins, M. J. Taylor, Interleukin-4 activated macrophages mediate immunity to filarial helminth infection by sustaining CCR3-dependent eosinophilia. *PLOS Pathog.* 14, e1006949 (2018).
- M. Osbourn, D. C. Soares, F. Vacca, E. S. Cohen, I. C. Scott, W. F. Gregory, D. J. Smyth, M. Toivakka, A. M. Kemter, T. le Bihan, M. Wear, D. Hoving, K. J. Filbey, J. P. Hewitson, H. Henderson, A. Gonzàlez-Ciscar, C. Errington, S. Vermeren, A. L. Astier, W. A. Wallace, J. Schwarze, A. C. Ivens, R. M. Maizels, H. J. McSorley, HpARI protein secreted by a helminth parasite suppresses interleukin-33. *Immunity* 47, 739–751.e5 (2017).
- A. Sharma, P. Sharma, L. Ganga, N. Satoeya, S. Mishra, A. L. Vishwakarma, M. Srivastava, Infective larvae of Brugia malayi induce polarization of host macrophages that helps in immune evasion. Front. Immunol. 9. 194 (2018).
- M. de Los Reyes Jiménez, A. Lechner, F. Alessandrini, S. Bohnacker, S. Schindela,
   A. Trompette, P. Haimerl, D. Thomas, F. Henkel, A. Mourão, A. Geerlof, C. P. da Costa,
   A. M. Chaker, B. Brüne, R. Nüsing, P.-J. Jakobsson, W. A. Nockher, M. J. Feige, M. Haslbeck,
   C. Ohnmacht, B. J. Marsland, D. Voehringer, N. L. Harris, C. B. Schmidt-Weber, J. E. Bieren,
   An anti-inflammatory eicosanoid switch mediates the suppression of type-2
   inflammation by helminth larval products. Sci. Transl. Med. 12, eaay0605 (2020).
- J. Esser-von Bieren, Immune-regulation and -functions of eicosanoid lipid mediators. Biol. Chem. 398, 1177–1191 (2017).
- J. W. McGinty, H.-A. Ting, T. E. Billipp, M. S. Nadjsombati, D. M. Khan, N. A. Barrett, H.-E. Liang, I. Matsumoto, J. von Moltke, Tuft-cell-derived leukotrienes drive rapid anti-helminth immunity in the small intestine but are dispensable for anti-protist immunity. *Immunity* 52, 528–541.e7 (2020).
- N. A. Barrett, O. M. Rahman, J. M. Fernandez, M. W. Parsons, W. Xing, K. F. Austen, Y. Kanaoka, Dectin-2 mediates Th2 immunity through the generation of cysteinyl leukotrienes. *J. Exp. Med.* 208, 593

  –604 (2011).
- M. M. M. Kaisar, M. Ritter, C. D. Fresno, H. S. Jónasdóttir, A. J. van der Ham, L. R. Pelgrom, G. Schramm, L. E. Layland, D. Sancho, C. P. da Costa, M. Giera, M. Yazdanbakhsh, B. Everts, Dectin-1/2-induced autocrine PGE2 signaling licenses dendritic cells to prime Th2 responses. PLoS Biol. 16, e2005504 (2018).
- Y.-G. Kim, K. G. S. Udayanga, N. Totsuka, J. B. Weinberg, G. Núñez, A. Shibuya, Gut dysbiosis promotes M2 macrophage polarization and allergic airway inflammation via fungi-induced PGE2. Cell Host Microbe 15. 95–102 (2014).
- U. F. Prodjinotho, V. Gres, F. Henkel, M. Lacorcia, R. Dandl, M. Haslbeck, V. Schmidt, A. S. Winkler, C. Sikasunge, P. Jakobsson, P. Henneke, J. Esser-von Bieren, C. Prazeres da Costa, Helminthic dehydrogenase drives PGE 2 and IL-10 production in monocytes to potentiate Treg induction. *EMBO Rep.* 23, e54096 (2022).
- N. W. Brattig, A. Schwohl, A. Hoerauf, D. W. Büttner, Identification of the lipid mediator prostaglandin E2 in tissue immune cells of humans infected with the filaria *Onchocerca* volvulus. Acta Trop. 112, 231–235 (2009).
- K. Alhallak, J. Nagai, K. Zaleski, S. Marshall, T. Salloum, T. Derakhshan, H. Hayashi, C. Feng, R. Kratchmarov, J. Lai, V. Kuchibhotla, A. Nishida, B. Balestrieri, T. Laidlaw, D. F. Dwyer,

- J. A. Boyce, Mast cells control lung type 2 inflammation via prostaglandin E2-driven soluble ST2. *Immunity* **57**, 1274–1288.e6 (2024).
- A. Lechner, S. Bohnacker, J. Esser-von Bieren, Macrophage regulation & function in helminth infection. Semin. Immunol. 53, 101526 (2021).
- J. Esser-von Bieren, B. Volpe, D. B. Sutherland, J. Bürgi, J. S. Verbeek, B. J. Marsland, J. F. Urban, N. L. Harris, Immune antibodies and helminth products drive CXCR2dependent macrophage-myofibroblast crosstalk to promote intestinal repair. *PLOS Pathoa*. 11, e1004778 (2015).
- X.-F. Wang, H.-S. Wang, H. Wang, F. Zhang, K.-F. Wang, Q. Guo, G. Zhang, S.-H. Cai, J. Du, The role of indoleamine 2,3-dioxygenase (IDO) in immune tolerance: Focus on macrophage polarization of THP-1 cells. *Cell. Immunol.* 289, 42–48 (2014).
- X. Liu, N. Shin, H. K. Koblish, G. Yang, Q. Wang, K. Wang, L. Leffet, M. J. Hansbury,
   B. Thomas, M. Rupar, P. Waeltz, K. J. Bowman, P. Polam, R. B. Sparks, E. W. Yue, Y. Li, R. Wynn,
   J. S. Fridman, T. C. Burn, A. P. Combs, R. C. Newton, P. A. Scherle, Selective inhibition of IDO1 effectively regulates mediators of antitumor immunity. *Blood* 115, 3520–3530 (2010).
- F. Fallarino, U. Grohmann, C. Vacca, R. Bianchi, C. Orabona, A. Spreca, M. C. Fioretti, P. Puccetti, T cell apoptosis by tryptophan catabolism. *Cell Death Differ.* 9, 1069–1077 (2002).
- E. Dokmeci, L. Xu, E. Robinson, K. Golubets, K. Bottomly, C. A. Herrick, EBI3 deficiency leads to diminished T helper type 1 and increased T helper type 2 mediated airway inflammation: EBI3 deficiency leads to diminished Th1, increased Th2. *Immunology* 132, 559–566 (2011).
- B. Everts, R. Tussiwand, L. Dreesen, K. C. Fairfax, S. C.-C. Huang, A. M. Smith, C. M. O'Neill, W. Y. Lam, B. T. Edelson, J. F. Urban, K. M. Murphy, E. J. Pearce, Migratory CD103<sup>+</sup> dendritic cells suppress helminth-driven type 2 immunity through constitutive expression of IL-12. J. Exp.Med. 213, 35–51 (2016).
- K. Hildenbrand, S. Bohnacker, P. R. Menon, A. Kerle, U. F. Prodjinotho, F. Hartung, P. C. Strasser, D. A. M. Catici, F. Rührnößl, M. Haslbeck, K. Schumann, S. I. Müller, C. P. Da Costa, J. Esser-von Bieren, M. J. Feige, Human interleukin-12α and EBI3 are cytokines with anti-inflammatory functions. *Sci. Adv.* 9, eadg6874 (2023).
- 29. J. Esser-von Bieren, Eicosanoids in tissue repair. Immunol. Cell Biol. 97, 279-288 (2019).
- O. O. Oyesola, M. T. Shanahan, M. Kanke, B. M. Mooney, L. M. Webb, S. Smita, M. K. Matheson, P. Campioli, D. Pham, S. P. Früh, J. W. McGinty, M. J. Churchill, J. L. Cahoon, P. Sundaravaradan, B. A. Flitter, K. Mouli, M. S. Nadjsombati, E. Kamynina, S. A. Peng, R. L. Cubitt, K. Gronert, J. D. Lord, I. Rauch, J. von Moltke, P. Sethupathy, E. D. Tait Wojno, PGD2 and CRTH2 counteract type 2 cytokine–elicited intestinal epithelial responses during helminth infection. J. Exp. Med. 218, e20202178 (2021).
- C. Fork, A. E. Vasconez, P. Janetzko, C. Angioni, Y. Schreiber, N. Ferreirós, G. Geisslinger, M. S. Leisegang, D. Steinhilber, R. P. Brandes, Epigenetic control of microsomal prostaglandin E synthase-1 by HDAC-mediated recruitment of p300. *J. Lipid Res.* 58, 386–392 (2017).
- F. Liu, T. Romantseva, Y.-J. Park, H. Golding, M. Zaitseva, Production of fever mediator PGE2 in human monocytes activated with MDP adjuvant is controlled by signaling from MAPK and p300 HAT: Key role of T cell derived factor. Mol. Immunol. 128, 139–149 (2020).
- H. Sun, J. Lu, L. Wei, X. Wang, X. Xu, M. Dong, B. Huang, Histone acetyltransferase activity
  of p300 enhances the activation of IL-12 p40 promoter. *Mol. Immunol.* 41, 1241–1246
  (2004).
- F. Paradisi, R. Woolfson, K. F. Geoghegan, P. C. Engel, Identification of the residue responsible for catalysing regeneration of activity in the inactive glutamate dehydrogenase mutant D165N. FEBS Lett. 579, 2830–2832 (2005).
- J. Esser-von Bieren, B. Volpe, M. Kulagin, D. B. Sutherland, R. Guiet, A. Seitz, B. J. Marsland, J. S. Verbeek, N. L. Harris, Antibody-mediated trapping of helminth larvae requires CD11b and Fcy receptor I. J. Immunol. 194, 1154–1163 (2015).
- F. Karagiannis, S. K. Masouleh, K. Wunderling, J. Surendar, V. Schmitt, A. Kazakov, M. Michla, M. Hölzel, C. Thiele, C. Wilhelm, Lipid-droplet formation drives pathogenic group 2 innate lymphoid cells in airway inflammation. *Immunity* 52, 620–634.e6 (2020).
- L. Zhou, H. Zhuo, H. Ouyang, Y. Liu, F. Yuan, L. Sun, F. Liu, H. Liu, Glycoprotein non-metastatic melanoma protein b (Gpnmb) is highly expressed in macrophages of acute injured kidney and promotes M2 macrophages polarization. *Cell. Immunol.* 316, 53–60 (2017).
- W. N. Silva, P. H. D. M. Prazeres, A. E. Paiva, L. Lousado, A. O. M. Turquetti, R. S. N. Barreto, E. C. de Alvarenga, M. A. Miglino, R. Gonçalves, A. Mintz, A. Birbrair, Macrophage-derived GPNMB accelerates skin healing. Exp. Dermatol. 27, 630–635 (2018).
- A. Castoldi, L. B. Monteiro, N. van Teijlingen Bakker, D. E. Sanin, N. Rana, M. Corrado, A. M. Cameron, F. Hässler, M. Matsushita, G. Caputa, R. I. Klein Geltink, J. Büscher, J. Edwards-Hicks, E. L. Pearce, E. J. Pearce, Triacylglycerol synthesis enhances macrophage inflammatory function. *Nat. Commun.* 11, 4107 (2020).
- R. Song, L. Lin, Glycoprotein nonmetastatic melanoma protein B (GPNMB)
   ameliorates the inflammatory response in periodontal disease. *Inflammation* 42,
   1170–1178 (2019)
- A. K. Jha, S. C.-C. Huang, A. Sergushichev, V. Lampropoulou, Y. Ivanova, E. Loginicheva, K. Chmielewski, K. M. Stewart, J. Ashall, B. Everts, E. J. Pearce, E. M. Driggers, M. N. Artyomov, Network integration of parallel metabolic and transcriptional data

- reveals metabolic modules that regulate macrophage polarization. *Immunity* **42**, 419–430 (2015).
- T. Bouchery, R. Kyle, M. Camberis, A. Shepherd, K. Filbey, A. Smith, M. Harvie, G. Painter, K. Johnston, P. Ferguson, R. Jain, B. Roediger, B. Delahunt, W. Weninger, E. Forbes-Blom, G. Le Gros, ILC2s and T cells cooperate to ensure maintenance of M2 macrophages for lung immunity against hookworms. *Nat. Commun.* 6, 6970 (2015).
- J.T. Pesce, T. R. Ramalingam, M. M. Mentink-Kane, M. S. Wilson, K. C. El Kasmi, A. M. Smith, R. W. Thompson, A. W. Cheever, P. J. Murray, T. A. Wynn, Arginase-1–expressing macrophages suppress Th2 cytokine–driven inflammation and fibrosis. *PLoS Pathog.* 5, e1000371 (2009).
- R. T. Dackor, J. Cheng, J. W. Voltz, J. W. Card, C. D. Ferguson, R. C. Garrett, J. A. Bradbury, L. M. DeGraff, F. B. Lih, K. B. Tomer, G. P. Flake, G. S. Travlos, R. W. Ramsey, M. L. Edin, D. L. Morgan, D. C. Zeldin, Prostaglandin E₂ protects murine lungs from bleomycininduced pulmonary fibrosis and lung dysfunction. Am. J. Physiol. Lung Cell. Mol. Physiol. 301, L645–L655 (2011).
- Guideline: Preventive Chemotherapy to Control Soil-Transmitted Helminth Infections in At-Risk Population Groups (World Health Organization, 2017); http://ncbi.nlm.nih.gov/books/NBK487927/.
- J. Chen, Z. Gu, M. Wu, Y. Yang, J. Zhang, J. Ou, Z. Zuo, J. Wang, Y. Chen, C-reactive protein can upregulate VEGF expression to promote ADSC-induced angiogenesis by activating HIF-1α via CD64/PI3k/Akt and MAPK/ERK signaling pathways. Stem Cell Res. Ther. 7, 114 (2016).
- Y. Huang, H. Zhang, L. Wang, C. Tang, X. Qin, X. Wu, M. Pan, Y. Tang, Z. Yang, I. A. Babarinde, R. Lin, G. Ji, Y. Lai, X. Xu, J. Su, X. Wen, T. Satoh, T. Ahmed, V. Malik, C. Ward, G. Volpe, L. Guo, J. Chen, L. Sun, Y. Li, X. Huang, X. Bao, F. Gao, B. Liu, H. Zheng, R. Jauch, L. Lai, G. Pan, J. Chen, G. Testa, S. Akira, J. Hu, D. Pei, A. P. Hutchins, M. A. Esteban, B. Qin, JMJD3 acts in tandem with KLF4 to facilitate reprogramming to pluripotency. *Nat. Commun.* 11, 5061 (2020).
- C. T. Robb, Y. Zhou, J. M. Felton, B. Zhang, M. Goepp, P. Jheeta, D. J. Smyth, R. Duffin, S. Vermeren, R. M. Breyer, S. Narumiya, H. J. McSorley, R. M. Maizels, J. K. J. Schwarze, A. G. Rossi, C. Yao, Metabolic regulation by prostaglandin E<sub>2</sub> impairs lung group 2 innate lymphoid cell responses. *Allergy* 78, 714–730 (2023).
- M. Serra-Pages, R. Torres, J. Plaza, A. Herrerias, C. Costa-Farré, A. Marco, M. Jiménez,
   M. Maurer, C. Picado, F. de Mora, Activation of the prostaglandin E2 receptor EP2 prevents house dust mite-induced airway hyperresponsiveness and inflammation by restraining mast cells' activity. Clin. Exp. Allergy 45, 1590–1600 (2015).
- H. Miyoshi, K. L. VanDussen, N. P. Malvin, S. H. Ryu, Y. Wang, N. M. Sonnek, C. Lai, T. S. Stappenbeck, Prostaglandin E2 promotes intestinal repair through an adaptive cellular response of the epithelium. *EMBO J.* 36, 5–24 (2017).
- M. Fairweather, Y. I. Heit, J. Buie, L. M. Rosenberg, A. Briggs, D. P. Orgill, M. M. Bertagnolli, Celecoxib inhibits early cutaneous wound healing. J. Surg. Res. 194, 717–724 (2015).
- K. Iwanaga, M. Okada, T. Murata, M. Hori, H. Ozaki, Prostaglandin E<sub>2</sub> promotes wound-induced migration of intestinal subepithelial myofibroblasts via EP2, EP3, and EP4 prostanoid receptor activation. *J. Pharmacol. Exp. Ther.* 340, 604–611 (2012).
- K. Ganesh, A. Das, R. Dickerson, S. Khanna, N. L. Parinandi, G. M. Gordillo, C. K. Sen, S. Roy, Prostaglandin E2 induces oncostatin M expression in human chronic wound macrophages through Axl receptor tyrosine kinase pathway. *J. Immunol.* 189, 2563–2573 (2012).
- N. Markosyan, E. P. Chen, V. N. Ndong, Y. Yao, C. J. Sterner, L. A. Chodosh, J. A. Lawson,
   G. A. Fitzgerald, E. M. Smyth, Deletion of cyclooxygenase 2 in mouse mammary epithelial cells delays breast cancer onset through augmentation of type 1 immune responses in tumors. Carcinogenesis 32, 1441–1449 (2011).
- J. Esser, U. Gehrmann, M. D. Salvado, A. Wetterholm, J. Z. Haeggström, B. Samuelsson, S. Gabrielsson, A. Scheynius, O. Rådmark, Zymosan suppresses leukotriene C₄ synthase activity in differentiating monocytes: Antagonism by aspirin and protein kinase inhibitors. FASEB J. 25, 1417–1427 (2011).
- S. Ahmad, A. J. Ytterberg, M. Thulasingam, F. Tholander, T. Bergman, R. Zubarev,
   A. Wetterholm, A. Rinaldo-Matthis, J. Z. Haeggström, Phosphorylation of leukotriene
   C4 synthase at serine 36 impairs catalytic activity. J. Biol. Chem. 291, 18410–18418
   (2016).
- M. Carbonneau, L. M. Gagné, M.-E. Lalonde, M.-A. Germain, A. Motorina, M.-C. Guiot,
   B. Secco, E. E. Vincent, A. Tumber, L. Hulea, J. Bergeman, U. Oppermann, R. G. Jones,
   M. Laplante, I. Topisirovic, K. Petrecca, M.-É. Huot, F. A. Mallette, The oncometabolite
   2-hydroxyglutarate activates the mTOR signalling pathway. Nat. Commun. 7, 12700 (2016).
- P. J. Skuce, E. M. Stewart, W. D. Smith, D. P. Knox, Cloning and characterization of glutamate dehydrogenase (GDH) from the gut of *Haemonchus contortus*. *Parasitology* 118, 297–304 (1999).
- C. L. Montes, E. V. Acosta-Rodríguez, J. Mucci, E. I. Zuniga, O. Campetella, A. Gruppi, A Trypanosoma cruzi antigen signals CD11b+ cells to secrete cytokines that promote polyclonal B cell proliferation and differentiation into antibody-secreting cells. *Eur. J. Immunol.* 36, 1474–1485 (2006).

- F. Alessandrini, H. Schulz, S. Takenaka, B. Lentner, E. Karg, H. Behrendt, T. Jakob, Effects of ultrafine carbon particle inhalation on allergic inflammation of the lung. *J. Allergy Clin.* Immunol. 117, 824–830 (2006).
- L. E. Layland, J. Mages, C. Loddenkemper, A. Hoerauf, H. Wagner, R. Lang,
   C. U. Prazeres da Costa, Pronounced phenotype in activated regulatory T cells during a chronic helminth infection. *J. Immunol.* 184, 713–724 (2010).
- A. Lechner, F. D. R. Henkel, F. Hartung, S. Bohnacker, F. Alessandrini, E. O. Gubernatorova, M. S. Drutskaya, C. Angioni, Y. Schreiber, P. Haimerl, Y. Ge, D. Thomas, A. M. Kabat, E. J. Pearce, C. Ohnmacht, S. A. Nedospasov, P. J. Murray, A. M. Chaker, C. B. Schmidt-Weber, J. Esser-von Bieren, Macrophages acquire a TNF-dependent inflammatory memory in allergic asthma. J. Allergy Clin. Immunol. 149, 2078–2090 (2021).
- S. Bohnacker, F. Hartung, F. Henkel, A. Quaranta, J. Kolmert, A. Priller, M. Ud-Dean,
   J. Giglberger, L. M. Kugler, L. Pechtold, S. Yazici, A. Lechner, J. Erber, U. Protzer, P. Lingor,
   P. Knolle, A. M. Chaker, C. B. Schmidt-Weber, C. E. Wheelock, J. Esser-von Bieren, Mild
   COVID-19 imprints a long-term inflammatory eicosanoid- and chemokine memory in
   monocyte-derived macrophages. Mucosal Immunol. 15, 515–524 (2022).
- S. Anders, W. Huber, Differential expression analysis for sequence count data. Genome Biol. 11, R106 (2010).
- M. I. Love, W. Huber, S. Anders, Moderated estimation of fold change and dispersion for RNA-seq data with DESeq2. Genome Biol. 15, 550 (2014).
   N. Tarighi, D. Mangar, S. Rigger, L. Karnetädt, D. Thomas, N. Estrairás, P. M. Niking.
- N. Tarighi, D. Menger, S. Pierre, L. Kornstädt, D. Thomas, N. Ferreirós, R. M. Nüsing, G. Geisslinger, K. Scholich, Thromboxane-Induced α-CGRP release from peripheral neurons is an essential positive feedback loop in capsaicin-induced neurogenic inflammation. *J. Invest. Dermatol.* 139, 656–664 (2019).
- F. D. R. Henkel, A. Friedl, M. Haid, D. Thomas, T. Bouchery, P. Haimerl,
   M. de Los Reyes Jiménez, F. Alessandrini, C. B. Schmidt-Weber, N. L. Harris, J. Adamski,
   J. E. Bieren, House dust mite drives proinflammatory eicosanoid reprogramming and macrophage effector functions. *Allergy* 74, 1090–1101 (2019).
- J. Kolmert, A. Fauland, D. Fuchs, J. Säfholm, C. Gómez, M. Adner, S.-E. Dahlén, C. E. Wheelock, Lipid mediator quantification in isolated human and guinea pig airways: An expanded approach for respiratory research. *Anal. Chem.* 90, 10239–10248 (2018).
- T. Günther, J. M. Theiss, N. Fischer, A. Grundhoff, Investigation of viral and host chromatin by ChIP-PCR or ChIP-Seq analysis. *Curr. Protoc. Microbiol.* 40, 1E.10.1-1E.10.21 (2016).
- R Core Team, R: A language and environment for statistical computing (R Foundation for Statistical Computing, 2020); https://R-project.org/.
- H. Wickham, ggplot2: Elegant graphics for data analysis (Springer-Verlag, 2016); https://ggplot2.tidyverse.org.
- R. Stark, G. Brown, DiffBind: Differential binding analysis of ChIP-seq peak data (2011);
   http://bioconductor.org/packages/release/bioc/vignettes/DiffBind/inst/doc/DiffBind.pdf.
- S. Fishilevich, R. Nudel, N. Rappaport, R. Hadar, I. Plaschkes, T. Iny Stein, N. Rosen, A. Kohn, M. Twik, M. Safran, D. Lancet, D. Cohen, GeneHancer: Genome-wide integration of enhancers and target genes in GeneCards. *Database* 2017, bax028 (2017).
- P. Shannon, A. Markiel, O. Ozier, N. S. Baliga, J. T. Wang, D. Ramage, N. Amin,
   B. Schwikowski, T. Ideker, Cytoscape: A software environment for integrated models of biomolecular interaction networks. *Genome Res.* 13, 2498–2504 (2003).
- A. Pohl, M. Beato, bwtool: A tool for bigWig files. Bioinformatics 30, 1618–1619 (2014).
- D. R. Zerbino, N. Johnson, T. Juettemann, S. P. Wilder, P. Flicek, WiggleTools: Parallel processing of large collections of genome-wide datasets for visualization and statistical analysis. *Bioinformatics* 30, 1008–1009 (2014).
- Y. Zhang, U. Werling, W. Edelmann, "Seamless ligation cloning extract (SLiCE) cloning method" in *DNA Cloning and Assembly Methods, Methods in Molecular Biology*, S. Valla, R. Lale, Eds. (Humana Press, 2014), vol. 1116, pp. 235–244.
- A. de Marco, E. Deuerling, A. Mogk, T. Tomoyasu, B. Bukau, Chaperone-based procedure to increase yields of soluble recombinant proteins produced in E. coli. BMC Biotechnol. 7, 32 (2007).
- F. W. Studier, Protein production by auto-induction in high-density shaking cultures. Protein Expr. Purif. 41, 207–234 (2005).
- T. Chakrabortty, A. Mourao, Munich crystallography BAG, European Synchrotron Radiation Facility (2027), DOI: 10.15151/ESRF-ES-1409599116.
- 81. W. Kabsch, XDS. Acta Crystallogr. D Biol. Crystallogr. 66, 125-132 (2010).
- Collaborative Computational Project, Number 4, The CCP4 suite: Programs for protein crystallography. Acta Crystallogr. D Biol. Crystallogr. 50, 760–763 (1994).
- M. D. Winn, C. C. Ballard, K. D. Cowtan, E. J. Dodson, P. Emsley, P. R. Evans, R. M. Keegan, E. B. Krissinel, A. G. W. Leslie, A. McCoy, S. J. McNicholas, G. N. Murshudov, N. S. Pannu, E. A. Potterton, H. R. Powell, R. J. Read, A. Vagin, K. S. Wilson, Overview of the CCP 4 suite and current developments. Acta Crystallogr. D Biol. Crystallogr. 67, 235–242 (2011)
- 84. T. J. Smith, T. Schmidt, J. Fang, J. Wu, G. Siuzdak, C. A. Stanley, The structure of apo human glutamate dehydrogenase details subunit communication and allostery. *J. Mol. Biol.* **318**, 765–777 (2002).

## SCIENCE IMMUNOLOGY | RESEARCH ARTICLE

- L. C. Storoni, A. J. McCoy, R. J. Read, Likelihood-enhanced fast rotation functions. Acta Crystallogr. D Biol. Crystallogr. 60. 432–438 (2004).
- P. D. Adams, P. V. Afonine, G. Bunkóczi, V. B. Chen, I. W. Davis, N. Echols, J. J. Headd, L.-W. Hung, G. J. Kapral, R. W. Grosse-Kunstleve, A. J. McCoy, N. W. Moriarty, R. Oeffner, R. J. Read, D. C. Richardson, J. S. Richardson, T. C. Terwilliger, P. H. Zwart, *PHENIX*: A comprehensive Python-based system for macromolecular structure solution. *Acta Crystallogr. D Biol. Crystallogr.* 66, 213–221 (2010).
- P. Emsley, B. Lohkamp, W. G. Scott, K. Cowtan, Features and development of Coot. Acta Crystallogr. D Biol. Crystallogr. 66, 486–501 (2010).
- D. N. Mastronarde, Automated electron microscope tomography using robust prediction of specimen movements. J. Struct. Biol. 152, 36–51 (2005).
- N. Biyani, R. D. Righetto, R. McLeod, D. Caujolle-Bert, D. Castano-Diez, K. N. Goldie, H. Stahlberg, Focus: The interface between data collection and data processing in crvo-EM. J. Struct. Biol. 198. 124–133 (2017).
- S. Q. Zheng, E. Palovcak, J.-P. Armache, K. A. Verba, Y. Cheng, D. A. Agard, MotionCor2: Anisotropic correction of beam-induced motion for improved cryo-electron microscopy. *Nat. Methods* 14. 331–332 (2017).
- D. F. Keren, R. A. McDonald, J. S. Wassef, L. R. Armstrong, J. E. Brown, The enteric immune response to shigella antigens. *Curr. Top. Microbiol. Immunol.* 146, 213–223 (1989).
- Y. Z. Tan, P. R. Baldwin, J. H. Davis, J. R. Williamson, C. S. Potter, B. Carragher, D. Lyumkis, Addressing preferred specimen orientation in single-particle cryo-EM through tilting. Nat. Methods 14, 793-796 (2017).
- A. Grosche, A. Hauser, M. F. Lepper, R. Mayo, C. Von Toerne, J. Merl-Pham, S. M. Hauck, The proteome of native adult Müller glial cells from murine retina. *Mol. Cell. Proteomics* 15, 462–480 (2016).
- 94. J. R. Wiśniewski, A. Zougman, N. Nagaraj, M. Mann, Universal sample preparation method for proteome analysis. *Nat. Methods* **6**, 359–362 (2009).
- P. Navarro, M. Trevisan-Herraz, E. Bonzon-Kulichenko, E. Núñez, P. Martínez-Acedo,
   D. Pérez-Hernández, I. Jorge, R. Mesa, E. Calvo, M. Carrascal, M. L. Hernáez, F. García,
   J. A. Bárcena, K. Ashman, J. Abian, C. Gil, J. M. Redondo, J. Vázquez, General statistical framework for quantitative proteomics by stable isotope labeling. *J. Proteome Res.* 13, 1234–1247 (2014).
- D. M. Molina, A. Wetterholm, A. Kohl, A. A. McCarthy, D. Niegowski, E. Ohlson, T. Hammarberg, S. Eshaghi, J. Z. Haeggström, P. Nordlund, Structural basis for synthesis of inflammatory mediators by human leukotriene C4 synthase. *Nature* 448, 613–616 (2007).

Acknowledgments: We would like to thank S. Schindela, J. Grosch, M. Kulagin, L. Paulini, E. Hensch, and B. Schnautz for technical support and help with animal experimentation. We also would like to thank all blood donors for participation in this study. We would like to thank staff of the histology laboratory of the Dermatology Department, Klinikum rechts der Isar, and of the Department of Immunobiology, University of Lausanne, the Helmholtz Munich Genomics platform, and the EMBL Genomics Core Facility for technical support. We also would like to thank J. Böttcher for the supply of the  $EP2^{-/-}$  KO bones. We acknowledge the use of the x-ray crystallography platform at the Helmholtz Munich and V. Napolitano for support on x-ray data collection. We particularly would like to thank the animal caretakers of the Helmholtz Munich for animal husbandry. Funding: This work is financially supported by grants from the German Research Foundation [ES 471/2-3 (J.E.-v.B.), SPP2306; ES 471/7-1 (J.E.-v.B.), FOR2599; and ES 471/3-2 (J.E.-v.B.), 490846870-TRR355/1 TPB09 (J.E.-v.B. and C.P.d.C.)], the Swiss National Science Foundation grant 310030\_212312 (J.E.-v.B.), a Helmholtz Young Investigator grant VH-NG-1331 (J.E.-v.B.) by the Helmholtz Initiative and Networking Fund, the German Federal Ministry of Education and Research (BMBF) 01KA1610 (CYSTINET-Africa) (C.P.d.C.), and the Swedish Research Council DNR 2023-02312 (J.Z.H.) and DNR 2023-02305 (P.-J.J.). Author contributions: Conceptualization: J.E.-v.B. and S.B. Methodology: S.B., F.D.R.H., A.G., U.FP., A.S.D.M., S.B., T.T., D.T., R.G., M.U.-D., A.-C.K., A.Q., and A.M.K. Investigation: S.B., F.D.R.H., F.H., A.G., S.R., U.F.P., E.B.S., A.S.D.M., S.B., T.T., D.T., R.G., F.A., A.L., B.S., and A.M.K. Visualization: S.B., C.B., and M.U.-D. Funding acquisition: J.E.-v.B. Supervision: J.E.-v.B., C.P.d.C., M.J.F., M.S., E.P., S.M.H., C.E.W., and J.Z.H. Resources: A.G., P.-J.J., and D.V. Writing—original draft: J.E.-v.B. and S.B. Competing interests: J.E.-v.B. has submitted a patent application (WO2019193140A1) related to the immune regulatory effects of the H. polygyrus L3 larval homogenate and its components, including H. polygyrus GDH. J.E.-v.B., S.B., A.G., and A.S.D.M. have submitted a patent application (European patent application no. 24173451.6) related to the immune regulatory activities of heGDH. Data and materials availability: PDB ID of the x-ray structure (heGDH\_full length): 8QF0, PDB ID of the x-ray structure (heGDH $^{\Delta N}$ ): 8S3G, PDB ID of the EM structure (heGDH): 18456, PDB ID of the EM structure (heGDH<sup>C1365</sup>): 19693, and PDB ID of the EM structure (heGDH $^{\Delta N}$ ): 19692. Proteomic data are deposited in the database PRIDE (PXD044102), and ChIP-seq data are deposited in the database GEO (GSE259349). RNA-seq data are deposited in the database GEO (GSE259350). All other data needed to evaluate the conclusions in the paper are present in the paper or the Supplementary Materials. Materials (see table S4) can be purchased from the indicated suppliers or provided upon request.

Submitted 2 October 2023 Accepted 13 November 2024 Published 6 December 2024 10.1126/sciimmunol.adl1467